12-2014

Unlocking the Secrets of Multi-Flagellated Propulsion

Stefan Oma Nwandu-Vincent
University of Tennessee - Knoxville, snwanduv@vols.utk.edu

To the Graduate Council:

I am submitting herewith a dissertation written by Stefan Oma Nwandu-Vincent entitled "Unlocking the Secrets of Multi-Flagellated Propulsion." I have examined the final electronic copy of this dissertation for form and content and recommend that it be accepted in partial fulfillment of the requirements for the degree of Doctor of Philosophy, with a major in Biomedical Engineering.

Mingjun Zhang, Major Professor

We have read this dissertation and recommend its acceptance:

WIlliam R. Hamel, Thomas T. Meek, Jindong Tan

Accepted for the Council:
Carolyn R. Hodges

Vice Provost and Dean of the Graduate School

(Original signatures are on file with official student records.)

Unlocking the Secrets of Multi-Flagellated Propulsion

A Dissertation Presented for the

Doctor of Philosophy

Degree

The University of Tennessee, Knoxville

Stefan Oma Nwandu-Vincent

December 2014

Dedication

This Dissertation is dedicated to my mother, Nkemdilim B. Ebube, for her emotional support throughout my Doctoral program.

ACKNOWLEDGEMENTS

I would like to thank Dr. Mingjun Zhang for serving as my Major professor throughout my program. I would like to also thank Dr. William R. Hamel and Dr. Jindong Tan for serving on my committee. I would also like to express my deep gratitude to Dr. Thomas T. Meek for serving as a mentor from my junior year of my undergraduate studies, writing my recommendation letter for graduate school and serving on my doctoral committee.

I would like to express my appreciation to Dr. Scott Lenaghan for his one on one help in teaching me various areas of my research including cell culture, microscope use and data analysis. I would also want to thank Dr. Ben Reese, for all his help in my research and being there for me to bounce ideas off. I extend my gratitude to every member of the Nano-Bio-systems and Nano-Bio-inspired Device Lab. I would like to thank the Tennessee Louis Stokes Alliance for Minority Participation (TLSAMP) for their support and resources in my undergraduate studies, the National Society of Black Engineers University of Tennessee Chapter (NSBE-UTK) for putting me in the position to learn leadership and professional skills. My deepest gratitude goes out to the Program for Excellence and Equity in Research (PEER), National Institute of Health for their support. Most of all I would like to thank God because without Him none of this would be possible.

Abstract

In this work, unique high-speed imaging platforms and an array of theoretical analysis methods are used to thoroughly investigate eukaryotic multi-flagellated propulsion using *Tritrichomonas foetus* as a test case. Through experimental observations through our imaging system with superior resolution and capture rate exceeding that of previous studies, it was discovered for the first time that the *T. foetus* employs a strategy similar to that of the "run and tumble" strategies found in bacteria and *Chlamydomona*s; it has two distinct flagellar beating patterns that result in two different body swimming motions, linear and turning swimming.

These two flagella patterns were then analyzed for the first time using two theoretical analysis methods that are often used to analyze uni-flagellated organisms; the Resistive Force Theory (RFT) and the Regularized Stokeslet Method (RSM). These theories were compared to uncover the more accurate method. Results showed that our modified-RFT model out-performed the RSM model. Due to these results, the quantitative analysis of the motion of each flagellum for both the swimming motions were carried out using the RFT method for the first time on a multi-flagellated cell, in both the 2-D and 3-D case.

Digital Holographic Microscopy was used to produce the 3-D trajectory of the *T.foetus* for the first time. Through this method it was possible to for the first time, quantitatively analyze the thrust and energy contributions of each flagella in each direction. We find out that the turning motion dissipates approximately half as much energy as the linear swimming motion which leads to the belief that the motion is more energy efficient. The energy results coupled with the thrust results show the highly coordinated nature of multi-flagellated propulsion. Through this RFT model, it was observed that the propulsive force of the *T.foetus* is comparable to that of other eukaryotes with varying numbers of flagella like the sperm and *Chlamydomonas*, suggesting that higher thrust generation is not necessarily the goal of multi-flagellated propulsion, but these

strategies result in greater maneuverability or sensing. Results from this study may serve as inspiration for biorobots due to the organism's ideal size and finely controlled multi-flagellated propulsion.

Table of Contents

List of Figures

Introduction

When the concept of swimming is discussed, we usually picture an organism swimming in an environment characterized by a high Reynolds number; mostly because our immediate environment is characterized by a high Reynolds number. So what is the Reynolds Number? It is a dimensionless number that is used to predict flow behaviors in different flow conditions. The Reynolds Number equation is $Re = \frac{\rho v L}{\mu}$, with v= the mean velocity of the object relative to the fluid, L=characteristic linear dimension, μ=Dynamic Viscosity of the fluid, and ρ=Density of the fluid. When the Reynolds number is multiplied by $\frac{vL}{vL}$, it becomes(1)

$Re = \frac{\rho v L}{\mu} = \frac{\rho v^2 L^2}{\mu v L} = \left(Inertia\ force\right) / \left(Viscous\ forces\right)$. This highlights the important relationship between Inertia forces and viscous forces that is inherent in the Reynolds number. In environments such as the one we live in, the inertia forces are far greater than the viscous forces, on the other hand microorganisms live in environments where the viscous forces dominate the inertia forces thus producing a low Reynolds number(10^{-5}~10^{-4}). In this sort of environment, the fluid passively responds to external forces; this means that a non-zero force on an object result in infinite acceleration(2). As a result, the total net force and torque of an object in low Reynolds number is always zero and that movement of the object at any moment is solely determined by the force exerted on it at that moment, and not by any previous forces(3). Reciprocal types of motion regardless of their speed do not lead to any net forward movement (3-5). These limitations make propulsion in this sort of environments very challenging and make research on how to overcome the increased viscous effects very important; especially in the case of developing medical bio-robots that will have to overcome these environments.

The first step in understanding propulsion in environment's characterized by low Reynolds number, is to carefully study the organisms that already inhabit and propel in that environment. Microorganisms have developed a vast amount of strategies to maneuver and navigate through this arduous environment. Some of these strategies are: the use of Pseudopodia in amoeba, gliding and twitching motility used by certain bacterium, the use of flagella by prokaryotic cells and the use of flagella and cillia by eukaryotic cells. The prokaryotic flagellum uses a motor to rotate the flagella and creating helical waves that propel the organism; the motor which is reversible, converts energy into useful mechanical motion similar to the motor found in cars and other mechanical devices. This energy derives from the gradients of ions across the cytoplasmic membrane(6). The reversible nature of the motor allows for the cell to change direction during swimming. The structure and function of the eukaryotic flagellum is significantly different from the prokaryotic flagellum. It consists of axonemes that are made up of a "9+2" structure; 9 pairs of microtubule doublets which surround two central single microtubules. The outer 9 doublet microtubules extend a pair of dynein arms to the neighboring microtubule. As opposed to the use of a motor in the prokaryote, the dynein arms of eukaryotes cause flagella beating; through ATP hydrolysis, a force is produced by the dynein arms and result in the microtubule doublets sliding against each other and the whole flagellum bending(7-9). The above mechanism usually results in planar motions that produce travelling sinusoidal wave.

Both prokaryotes and eukaryotes use both single and multi-flagellar configurations to effectively navigate their environment. A vast amount of research has been done on prokaryotes using multi-flagellated strategies to effectively generate propulsion; especially that of the peritrichous bacteria(10-12). These bacteria use a strategy that has been coined "run and

tumble". When all the flagella motors rotate in the same direction, the cell swims forward and is described to be in a "run" state. If one of these motors rotates in the opposite direction that the others rotate in, the forward motion is disrupted and often results in a chaotic 'tumble-like" motion which re-orients the cell prior to another "run" state. The production of two distinct motions from the same flagella structure is intriguing and it is presently unknown if this phenomenon is only restricted to prokaryotic cells or is a universal characteristic for microorganisms. Significantly less is known about multi-flagellar propulsion strategies in eukaryotic cells. Of the few studies conducted on this topic, a good amount of research has been conducted on the biflagellate algae *Chlamydomonas* (13-15). It has been discovered that this algae shows swimming behaviors similar to that of the "run and tumble" behavior exhibited by peritrichous bacteria. The *Chlamydomonas* can vary the beating frequencies of its flagella so that they can switch between synchronous and asynchronous beating resulting in cells alternating from straight swimming to sudden reorientations (16). The lack of in-depth research in the area of multi-flagellar propulsion of eukaryotic cells makes its study essential. A complete first of its kind quantitative analysis of flagella kinematics, flagella mechanical properties, and thrust generation techniques of the cell will be implemented to investigate multi-flagellar propulsion of eukaryotic cells. A unique combination of high-speed high-contrast video microscopy, nanoscale imaging and nanoindentation, plus detailed theoretical analysis will be employed to accomplish this goal. Various theoretical techniques have been used to calculate flagella and cilia aided swimming. The first quantitative analysis of swimming microorganisms was done by Taylor(17). That paper assumed the flagellum to be a two-dimensional, small amplitude sheet. From this crude approximation, Hancock built on it forming more realistic models and placing a distribution of stokeslets and doublets along the length of the flagellum. This method is often

referred to as using the slender-body theory(18) (SBT). Based on the SBT, Gray & Hancock(19) developed the resistive-force theory (RFT) which only account for the near field hydrodynamic effect along the flagella, in essence it is a near field approximation. Lighthill improved on Gray & Hancock's work by deriving more accurate drag coefficients(20)**.** Both SBT and RFT do not take into effect the hydrodynamic effects of the body on the flagellum. Johnson and Brokaw(21) compared The Resistive Force Theory to The Slender Body Theory and concluded that even though SBT was more accurate, the RFT was satisfactory for organisms with small cell bodies. The RFT has served as the basis for most uni-flagellated propulsive studies due to its low computational effort in relation to the SBT. Brokaw validated the RFT by analyze the planar motions of the sperm tail while comparing the results to average experimental propulsive velocities, this was followed by other works which used the RFT to analyze sperm propulsion(22). Improvements to the SBT where conducted by Higdon; that work accounted for the head-flagellum interaction that the RFT ignored. Cortez et al presented the regularized stokeslet as a more accurate alternative as it removed singularities from the distributions of the stokeslet and this method has been applied to various uni-flagellated cells(23, 24).

As implied previously, all of studies mentioned were on a uni-flagellate cell, scarce work has been done on multi-flagellated cells where a comparison study similar to that of Johnson and Brokaw(21) would greatly aid the field of multi-flagellated propulsion because the cell body-flagella and flagella-flagella hydrodynamic effects are more pronounced in this case. The regularized stokeslet method uses smoothed point forces at each stokeslet location to calculate the flow induced by a point on the flagellum(23, 25-27). Various researchers have used these theories to quantitatively analyze these microorganisms in 2-D, but none of them have applied it

to a multi-flagellated cell. In this work we apply these theories to the multi-flagellate *Tritrichomonas foetus*.

Tritrichomonas foetus is a multi-flagellated microorganism found in the urogenital tract of cattle and the etiological agent of bovine trichomoniasis. Trichomoniasis in cattle typically causes vaginitis, abortion, and infertility in cattle and the financial burden associated with the diagnosis and treatment of this pathogen is significant (28-31). Often, an infected herd can result in up to a 35 percent decrease in profitability per cow (32). In addition to causing disease in cattle, *T. foetus* has also been linked to large-bowel chronic diarrhea in cats, although it is unknown how cats come into contact with the parasite (28, 29, 33). Morphologically, the cell is characterized by a spindle shaped body with three flagella extending from the anterior region of the cell, and a recurrent flagellum originating near the anterior, extending towards the posterior with intermittent attachments to the cell body. The intermittent attachment of the recurrent flagella to the cell body leads to the formation of the undulating membrane, which terminates at the posterior region of the cell leaving the free posterior flagellum (29). Although *T. foetus* has been well-studied, much is still unknown about the exact swimming mechanisms.

Multi-flagellated propulsion strategies used by microorganisms serve as ideal case studies to use as inspiration for a targeted drug delivery bio-robot. Targeted drug delivery with the aid of micro-robots has been identified as a promising breakthrough in the diagnosis and treatment of diseases ranging from cancer to broken limbs. For these bio-robots to be effective, an efficient propulsion mechanism will be needed for adequate maneuverability of the rugged environment of the human body. Using organisms already existing in environments similar to that of the body is ideal; since the organisms already target and attach to specific cells similarly to the way a targeted drug delivery bio-robot would preferably function. Numerous studies are being done

with uni-flagellated bio-robots; having multiple flagella serves to increase the control of directionality of the organism which is preferred for optimum maneuverability. So a comprehensive study of eukaryotes using multi-flagellar configurations to propel and maneuver in their environment serves both a major purpose in possibly diagnosing certain diseases and also developing effective therapeutic approaches to existing ailments.

Research Objective

In this study, we examine micro-organism propulsion in low Reynolds number environments. We focus on multi-flagellated propulsion strategies of eukaryotic cells due to the lack of in-depth research in this area. We examine the highly motile *Tritrichomonas foetus*; we examine their swimming mechanism and its resultant propulsive and navigative effects along with mechanical properties of their flagella to thoroughly understand their locomotion with hopes of inspiring future bio-robot applications. The specific aims of the study are listed below:

Specific Aim 1

Comprehensively analyze the multi-flagellated propulsion strategies used by *T.foetus*; quantitatively analyze the flagella kinematics, mechanical properties, and thrust generation techniques of the cell. Our unique setup, the Cytoviva™ microscopic platform coupled with a high-speed PIV camera, will be used for visualization of the cell along with the ImageJ software system to acquire positional data of the cell. An Asylum MFP/3D atomic force microscope (AFM) will be used for Nanoscale imaging and nanoindentation to elucidate the Young's modulus of the flagella. The Resistive Force Theory (RFT) will be employed to generate propulsive forces of the cell.

Specific Aim 2

Compare and contrast leading theoretical analysis techniques used to generate propulsive forces of flagellates. Compare the resistive force theory (RFT) and the Regularized Stokeslet Method (RSM) and discuss their accuracy in predicting multi-flagellated propulsion.

Specific Aim 3

Quantitatively Analyze *T.foetus* in 3-D by generating the 3-D trajectory of the body and flagella using Digital Holography (DHM) and analyzing flagella and body kinematics with a 3-D RFT model

Significance of Proposed Work

The microorganisms studied are lethal pathogens; their ability to maneuver within the body in very treacherous environments is vital to their pathogenesis, which is not thoroughly understood. We examine how these cells are able to navigate their environments using well-coordinated multi-flagella configurations. This work will lead to major insights into the biology of these organisms and aid in understanding general principles of multi-flagellated propulsion. Also insights from this study will serve as inspiration for medical bio-robot designs; due to the fact that the bio-robots would be of similar size and will have to navigate similar environments as the microorganism.

Chapter 1
Comprehensively analyze the multi-flagellated propulsion strategies used by *T.foetus*

A version of this chapter was originally published by Scott Lenaghan, Stefan Nwandu-Vincent, Ben Reese and Mingjun Zhang:

Lenaghan S. C., Nwandu-Vincent S, Reese BE, Zhang M. (2014) Unlocking the secrets of multi-flagellated propulsion: drawing insights from *Tritrichomonas foetus*. *J. R. Soc. Interface* 20131149.

Nwandu-Vincent co-wrote the paper, performed model analysis, performed video acquisition and analysis. Dr. Lenagahan co-wrote the paper, co-performed video analysis and co-designed the research. Dr. Zhang co-designed the research and provided analytical tools (CytoViva and AFM.Nanoindentor) for research. Reese performed analysis with Nano-indentor, co-performed video analysis and co-wrote the paper.

Abstract

In the present work, a high-speed imaging platform and a resistive force theory (RFT) based model were applied to investigate multi-flagellated propulsion, using *Tritrichomonas foetus* as an example. We discovered that *T. foetus* has distinct flagellar beating motions for linear swimming and turning, similar to the "run and tumble" strategies observed in bacteria and *Chlamydomonas*. Quantitative analysis of the motion of each flagellum was achieved by determining the average flagella beat motion for both linear swimming and turning, and using the velocity of the flagella as inputs into the RFT model. The experimental approach was used to calculate the curvature along the length of the flagella throughout each stroke. It was found that the curvature of the anterior flagella do not decrease monotonically along their lengths, confirming the ciliary waveform of these flagella. Further, the stiffness of the flagella was experimentally measured using nanoindentation, allowing for calculation of the flexural rigidity of *T. foetus's* flagella, 1.55×10^{-21} N·m^2. Finally, using the RFT model, it was discovered that the propulsive force of *T. foetus* was similar to that of sperm and *Chlamydomonas*, indicating that multi-flagellated propulsion does not necessarily contribute to greater thrust generation, and may have evolved for

greater maneuverability or sensing. The results from this study have demonstrated the highly coordinated nature of multi-flagellated propulsion and have provided significant insight into the biology of *T. foetus*.

Introduction

For microorganisms, which reside at low Reynolds number (10^{-5}~10^{-4}), reciprocal types of motion are incapable of generating net forward propulsion (3-5). In order to overcome this limitation, microorganisms have evolved highly specialized propulsive structures, such as cilia and flagella, to generate non-reciprocal traveling waves. In the case of prokaryotic flagella, a rotary motor drives the flagella resulting in a helical waveform, which acts as a propeller to move the microorganism (7). Eukaryotic flagella, however, are able to generate planar waveforms from the sliding of microtubules along the length of the flagella (7-9). In addition to these differing flagella structures, prokaryotes and eukaryotes have adopted both single and multi-flagellar configurations to generate propulsion. While much research has been conducted on multi-flagellated propulsion and maneuverability in prokaryotes, specifically the "run and tumble" strategy of peritrichous bacteria (10-12), fewer studies have examined multi-flagellated propulsion in eukaryotes, with the exception of the biflagellated algae *Chlamydomonas* (13-15). In fact, researchers have recently discovered that *Chlamydomonas* exhibits a similar "run and tumble" behavior, where cells switch from nearly straight swimming to abrupt large reorientations (16). Previously, we developed a high-speed imaging platform that allowed for increased resolution of flagella, allowing for detailed qualitative analysis of propulsion in the octo-flagellated eukaryote *Giardia lamblia* (34, 35). In the present work, we combined the previously developed high-speed imaging platform with a state-of-the-art nanoindenter and resistive force theory (RFT), to quantitatively analyze multi-flagellated propulsion using *Tritrichomonas foetus* as a test case.

Unlike the bilaterally symmetric multi-flagellar arrangement of *Chlamydomonas* and *Giardia*, the quadri-flagellated trophozoites of *T. foetus* have four flagella that originate at the anterior pole, with the single recurrent flagellum curving back along the cell body, attaching at several points to form the undulating membrane (**Fig. 1A**) (36-43). The three anterior flagella (one free and two stalked at their base) extend freely from the anterior pole. Previous studies have revealed that the cytoskeleton (i.e., axostyle and costa) of *T. foetus* remains rigid throughout the entirety of its swimming motion (44), as opposed to other trichomonads (45) and *Giardia* (34), in which body flexion can be observed. Since the cell body of *T. foetus* is shown to be rigid during swimming, the propulsive forces necessary for swimming must be the result of flagellar beating (44), making this microorganism ideally suited for the study of multi-flagellated propulsion.

In order to comprehensively analyze multi-flagellated propulsion in *T. foetus*, quantitative analyses of the flagella motion, including kinematics and curvature changes, mechanical properties of the flagella, and thrust generation were conducted. Quantitative data for the movement of the cell body and flagella was obtained using the increased resolving capabilities of the Cytoviva™ microscopic platform, coupled with a high-speed PIV camera. While previous attempts have been made to characterize the flagella beating of *T. foetus*, the low speed of capture, 30 fps, and poor resolution used in these studies were not able to fully account for the complex dynamics of their rapid motion (44, 46). Using the improved spatiotemporal resolution of this platform, two distinct

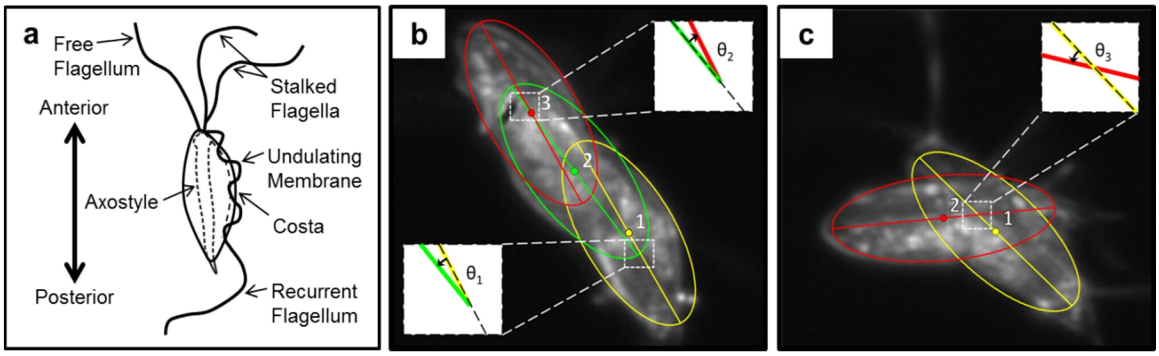

Fig. 1.1 Morphological diagram of *T. foetus* and motion of the cell body during linear swimming and turning. A) Morphology of *T. foetus* trophozoite, demonstrating the positioning of the four flagella, anterior and posterior poles, and internal cytoskeletal structures. B) Motion of the cell body during linear swimming, showing its ability to correct for angular changes in consecutive beats resulting in an overall linear path. Ellipses have been superimposed over the body at the initial and final positions of each beat to identify the center of mass of the cells, marked as points 1-3.The change in angle over the first beat (θ_1) with respect to the initial orientation (dotted line) was -13.74°. After the second beat, the change in angle (θ_2) was 13.74°, which resulted in a net angular change of 0° over two beats. C) The change in angle of the cell body during turning (θ_3) was 32.8°, and since the body does not spin around the longitudinal axis during this beat, no angular correction takes place in consecutive beats.

flagella beating patterns were discovered for either linear swimming or abrupt changes in orientation (termed turning). These distinct patterns demonstrate sophisticated coordination and control, and indicate specific roles for the anterior and recurrent flagella in propulsion. In addition, the ability of the cell to rapidly alter its flagella beating pattern for linear swimming and turning, suggests a eukaryotic "run and tumble" behavior, similar to *Chlamydomonas*. Further, nanoindentation was used to determine mechanical properties of the flagella, while curvature changes along the length of the flagella was calculated for both linear and turning motions. Quantitative analysis of the curvature of the flagella confirmed that *T. foetus* exhibits two distinct flagellar beating patterns. Additional analyses using the RFT model revealed that the observed rotation of the cell along its longitudinal axis in linear swimming allows the cell to maintain a linear trajectory. Using this model, we were also able to calculate the thrust generated by each flagellum and compare the propulsive force of *T. foetus* to other microorganisms employing both single and multi-flagellated swimming strategies.

Results

Experimental Analysis

Using the integrated experimental platform, the motion of *T. foetus* trophozoites was captured at 167 fps, 40 times greater than the reported beating frequency of the anterior flagella (44, 46). Analysis of the swimming motions from > 100 cells revealed two distinct flagella beating patterns resulting in two different trajectories of the cell body, recognized as either linear swimming or turning. It was discovered that the cell moves in a linear trajectory (**Fig. 1.1B**) by using the rotation of the cell about its longitudinal axis (termed spinning) to offset the angular changes from consecutive beats. The turning motion was found to generate a large angular change from sequential beats, with no observable spinning. When the cell used the turning motion, it was able to make more radical and abrupt changes to its orientation and trajectory

(**Fig. 1.1C**). To confirm that the two swimming motions were distinct, quantitative analyses of the flagella dynamics for both motions were further characterized.

As illustrated in previous studies, the anterior flagella beating motion can be separated into two time-dependent phases, the active and recovery strokes (44, 46). During the active stroke, the anterior flagella extend out in front of the cell body resulting in a backwards motion of the cell, similar to *Chlamydomonas* (47). The recovery stroke immediately follows the active stroke, as the anterior flagella are pulled back towards the cell body, propelling the cell forward. Since the active stroke was obscured by the cell body, only the motion during the recovery stroke was considered in this work. It was determined that the recovery stroke for linear swimming was 32% ($p = 6.6x10^{-11}$) longer in duration and that the cell traveled 27% ($p = 0.018$) farther during linear swimming when compared to turning (**Table 1.1**). The angular change of the cell body during the turning stroke was also found to be 2.4 times larger ($p = 0.005$) despite the shorter duration of its beat (**Table 1.1**). Additionally, linear swimming cells were found to spin ~180° during a single beat, while in turning, there was no detectable spinning, as can be seen by the position of the axostyle in **Fig. 1.2A&C**. Due to the spinning observed in linear swimming, no difference in the beating pattern of the recurrent flagellum was observed. Considering that the cytoskeleton (i.e., axostyle and costa) of *T. foetus* remains rigid during the entire swimming motion (44), it was determined that the forces generating the two distinct motions of the cell body in linear swimming and turning were the result of altered flagella beating patterns.

In order to correlate the motion of the cell body with that of the flagella, traces of the recovery stroke for all four flagella were generated for both linear swimming and turning (**Fig. 1.2A&C**). Using a method similar to (48), "point clouds" were generated for the flagella of 10 distinct

Table 1.1. Data Obtained from Experimental Analysis of T. foetus During Linear Swimming and Turning

Length of body (µm)	14.63 ± 1.30	
Width of body (µm)	6.73 ± 1.00	
Eccentricity of body	0.89	
Length of flagella (µm)	12.33 ± 1.44	
Viscosity of Water ($N•s/m^2$)	$1x10^{-3}$	
Young's Modulus (GPa)	11.96 ± 3.51	
Recovery Stroke	Linear	Turning
Duration (s)	0.326 ± 0.027	0.223 ± 0.043
Distance Traveled (µm)	6.86 ± 1.18	5.01 ± 1.79
Angular Change (°)	13.74 ± 4.26	32.84 ± 12.09
Duration of Free Flagella Beat (ms)	97 ± 9.7	85 ± 12.24
Duration of First Stalked Flagella Beat (ms)	105 ± 26.2	130 ± 17.25
Duration of Second Stalked Flagella Beat (ms)	125 ± 18.3	131 ± 16.72

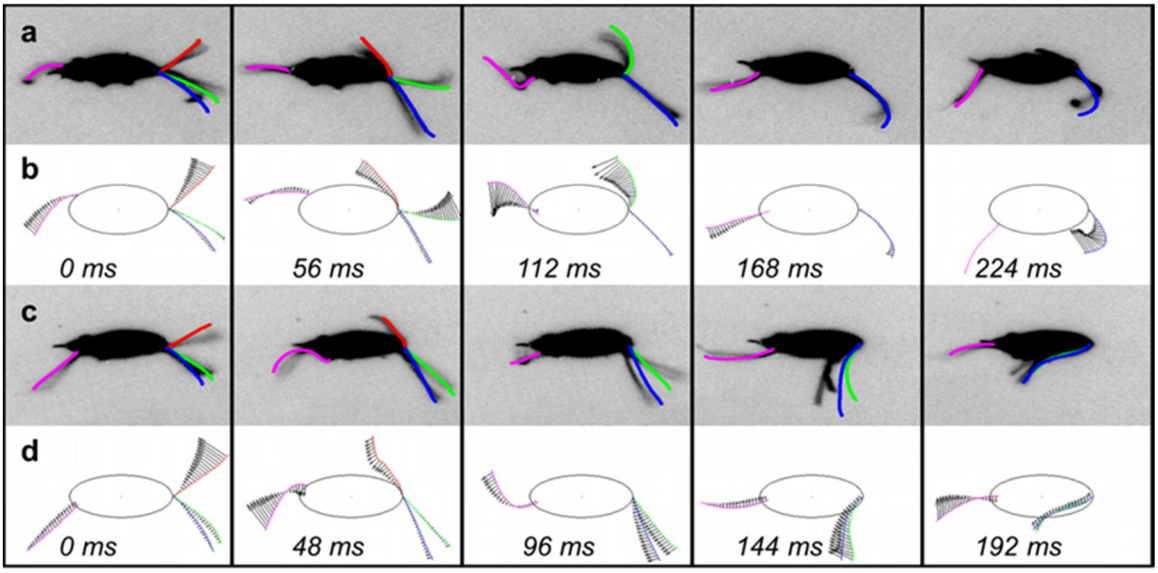

Fig. 1.2 Comparison of flagella motion during linear swimming and turning in the body-fixed frame. A) The average flagella traces for linear swimming were overlaid onto inverted images of a single cell to demonstrate the fit of the average traces. B) The polynomial fits of the flagella during straight swimming, with the force vectors indicated. C) The average flagella beat motion during turning overlaid onto inverted images of a typical turning cell. D) The polynomial fits of the flagella during turning, with the force vectors indicated. As clearly illustrated in the Fig., the two stalked flagella beat simultaneously during turning, with vectors oriented in the same direction with similar magnitudes. For linear swimming, the stalked flagella beat over separate time intervals. In all images, red indicates the free flagellum, green represents the first stalked flagellum, blue represents the second stalked flagellum, and pink represent the recurrent flagellum

linear swimming cells and 10 distinct turning cells during the recovery stroke. Polynomials were fit to the point clouds at 10 evenly spaced time intervals to generate an average flagella beat pattern for both linear swimming and turning. When comparing the duration of each anterior flagellum beat for turning, it was determined that the free flagellum beat with a shorter duration than the stalked flagella (**Table 1.1**). Additionally, stalked flagella 1 and 2 (referred to as stalked 1 and stalked 2 from this point forward) were found to beat together, resulting in the same duration throughout the turning motion (**Table 1.1**). In contrast, for linear swimming, propulsion from each flagellum occurred over a different time interval. Another key difference between the anterior flagella during linear swimming and turning was that the two stalked flagella beat on opposite sides of the body for linear swimming, having opposing angular contributions, while they beat on the same side of the body and sum together to generate a larger angular change during turning (**Fig. 1.2A&C**). Commensurate with this change, the two stalked flagella appeared to have a much more rigid beating form during turning.

In order to analyze the curvature changes in the average flagella at each time point, over the length of the flagella, each flagella was divided into 10 distinct regions. The first region spanned from the point of exit from the cell body to 10% of the flagella length, followed by further segmentation for every 10% increase in length (10-20%, 20-30%, etc.). The curvature of these regions was calculated at each time point using the method of Okuno et al. (49). Briefly, by taking the angle formed by two tangents at the points before and after the point of interest and dividing it by the length of that section, curvature was calculated. In **Fig. 1.3**, a color gradient was used to represent the degree of curvature in the different regions along the length of the flagella. Quantitative analysis of the curvature change revealed similar trends to those observed from the video microscopy analysis. In both linear swimming and turning, the free flagella has

little curvature at the first time instant, followed by a gradual increase in the first 20% at the second time interval. More pronounced curvature is observed for the rest of the free flagella beat, with the curvature increasing along the length of the flagella. The most obvious difference between linear swimming and turning is the lack of curvature in both stalked 1 and 2 throughout the entire beat cycle. In linear swimming, both of the stalked flagella have regions where the curvature exceeds 40°; however, during turning neither stalked flagella exceeds 30°. In fact for the first 97 ms of turning, the stalked flagella have almost no curvature. This is in opposition to linear swimming, where stalked 1 has significant curvature at 85 ms. Analysis of the curvature also supports the observation from video microscopy that during linear swimming the anterior flagella beat out of phase with each other, while stalked 1 and 2 beat in phase for turning. Further, since the curvature of the anterior flagella do not decrease monotonically along their lengths, this analysis demonstrates that they move with a ciliary waveform rather than with a sinusoidal beat (50, 51). Analysis of the recurrent flagella between linear swimming and turning did not reveal any significant differences in the magnitude of curvature, which was not surprising due to the similarity of the beats between the two motions. In addition to curvature, this analysis highlights the timing and coordination necessary for *T. foetus* to effectively utilize these two distinct beating patterns for effective propulsion. To further characterize the motion of the flagella between the two beating patterns, quantitative analyses of the flagella mechanics were conducted.

Mechanics Analysis

While several studies have used atomic force microscopy (AFM) to image various protozoa (52-55), none have applied nanoindentation to experimentally determine the mechanical properties of the flagella of these microorganisms. Using nanoindentation, we determined that the Young's modulus for the flagella of *T. foetus* was 11.96 ± 3.51 GPa (**Fig. 1.4**). Considering

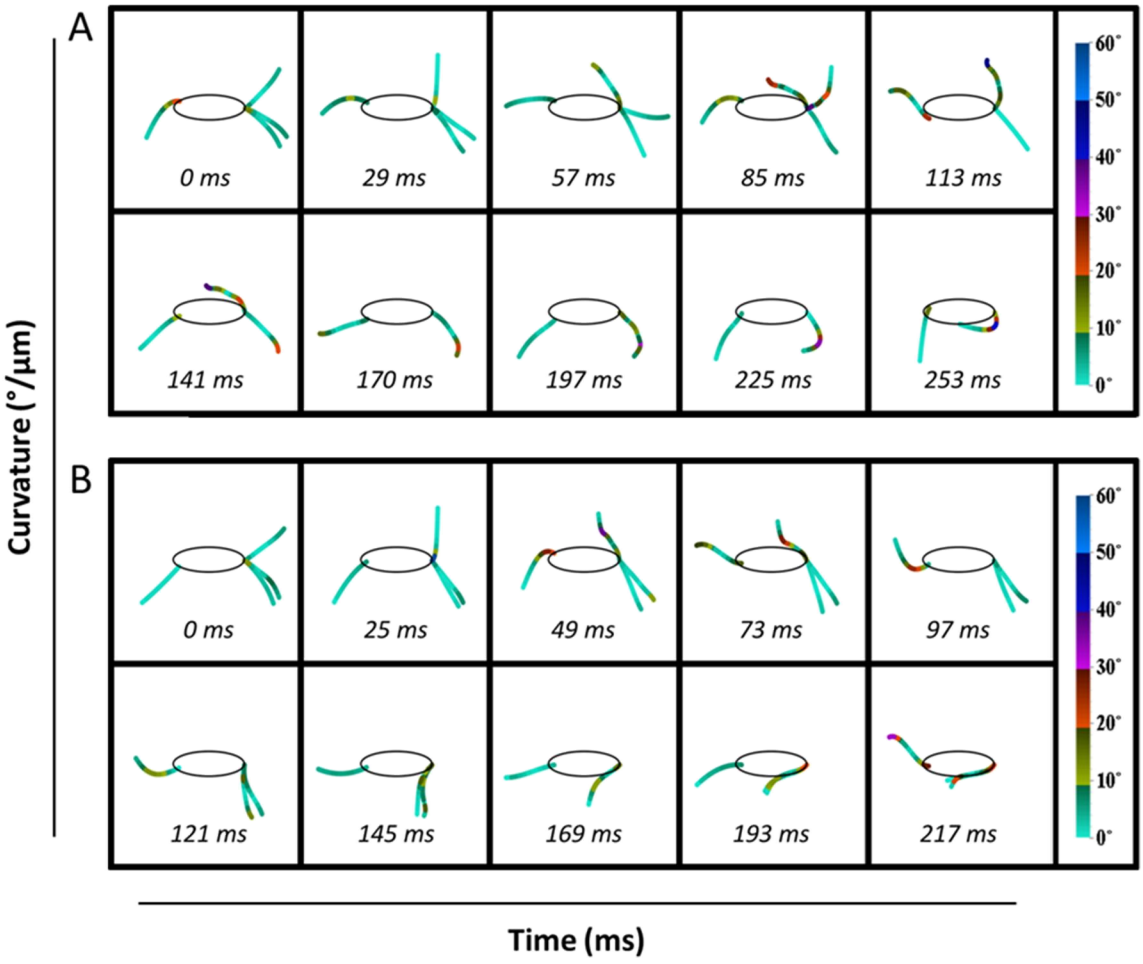

Fig. 1.3 Curvature changes along the length of each flagellum during the entire recovery stroke of linear swimming and turning. The zero point of each flagellum was the point of exit from the cytoplasm. Curvature was then calculated at equally distributed intervals along the length of the flagella (10% increments). The magnitude of curvature at each increment is shown by the gradient color bar. When comparing the changes in curvature between linear swimming (A) and turning (B), it is apparent that differences exist between the strokes, both in the magnitude of the curvature and the time phase of bending.

that the cells were fixed with glutaraldehyde prior to analysis, the measured modulus is expected to be higher than in the natural biological state. Unfortunately, limited data exists on the extent to which fixation effects Young's modulus values obtained from nanoindentation. In a recent study, the stiffness of cartilage was found to increase by one order of magnitude after fixation with paraformaldehyde (56); however, it is unknown the degree to which the stiffness of flagella will change after fixation.

Assuming the same moment of inertia (I) as a typical (9 + 2) eukaryotic axoneme (49), the flexural rigidity of the flagella in *T. foetus* was estimated to be 1.55×10^{-21} N·m^2, within the range of other eukaryotic flagella. While similar values have been reported for sperm flagella (0.3-5.8×10^{-21} N·m^2) (57), when compared to typical (9 +2) cilia (3-13×10^{-18} N·m^2) (58) and bacterial flagella (1.0×10^{-14} N·m^2) (59), the flagella of *T. foetus* are considerably more flexible. Recent studies have reported that primary mammalian cilia (9 + 0), however, are considerably more flexible (1.4-3.9×10^{-23} N·m^2) than the flagella of *T. foetus*, which would be expected due to the lack of central pair microtubules in primary cilia (60). After obtaining a value for the flexural rigidity of the flagella and the curvature change along the length of the flagella, it was possible to calculate the bending moments along the length of the flagella. Briefly, by multiplying the flexural rigidity by the curvature at a particular point on the flagella the bending moments were calculated; however, the trends are identical to those shown for curvature alone, thus only curvature was shown in **Fig. 1.3**. Next, a dynamics model was created to further characterize the differences in these strokes, and identify the role of each flagellum in propulsion.

Dynamics Analysis of Swimming

Model validation

The input to the model was the flagella traces obtained from the experimental platform; however, to ensure the same distance between points along the length of the flagella,

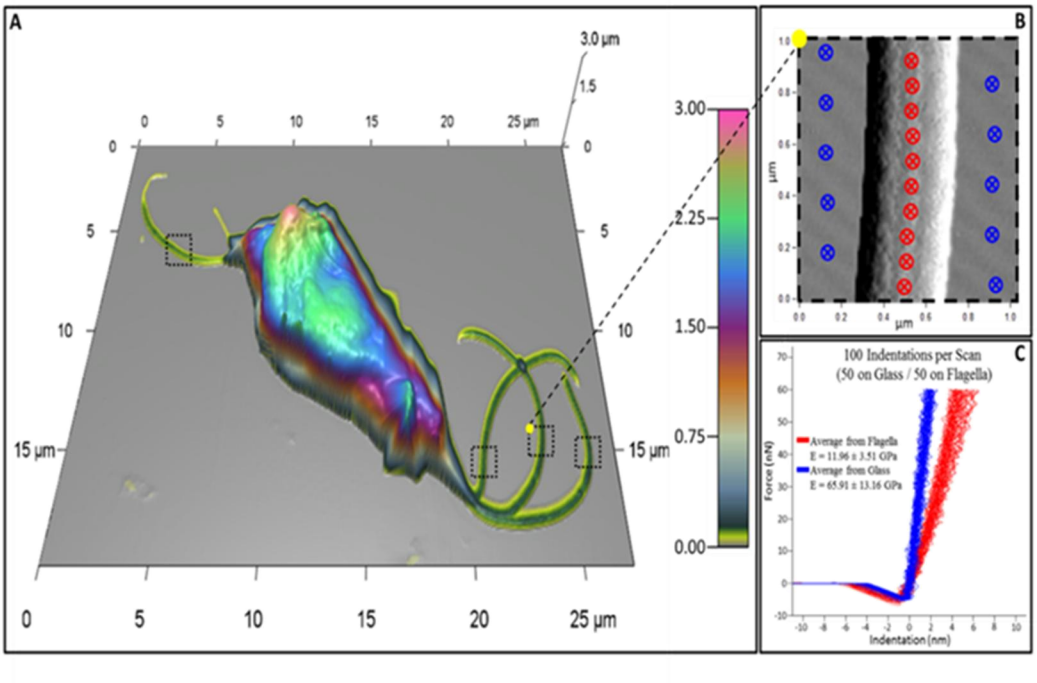

Fig. 1.4 Determination of the Young's modulus for *T. foetus's* flagella using nanoindentation . A) A 3D topographical image of *T. foetus* used to visualize the location and orientation of each flagellum. B) A 1µm^2 scan over the selected region used for the placement of indentation points (20 total, 10 on glass and 10 on flagellum) shown in blue (glass) and red (flagellum). C) Resulting force versus indentation curves (blue:glass, red:flagella) from the selected points in (B), along with the calculated averages of Young's modulus for both glass and flagellum (65.91 ± 13.16 GPa and 11.96 ± 3.51GPa).

polynomials were fit to the flagella traces (**Fig. 1.2B&D**). As shown in **Fig. 1.2**, the polynomial fits accurately represent the average flagella traces, and therefore can be used to calculate the flagellar forces. The first step in determining the forces generated by the flagella during both linear swimming and turning was to determine the ratio of the tangential and normal drag coefficients on the flagella (C_T/C_N). Considering the complexity associated with modeling a multi-flagellated microorganism, we chose to set the C_T/C_N ratio to 0.5, the optimum ratio for a smooth cylinder (61). Previous studies have found that C_T/C_N ratios range from 0.44-0.7 for microorganisms with either cilia or flagella as the primary motile structure (13, 62-68). The only microorganisms known to have a C_T/C_N ratio outside of this range, and > 1, are the hispid flagellates such as *Euglena* (69). In these microorganisms, the flagella are modified with mastigonemes, stiff filaments that extend perpendicular to the flagella surface, providing the necessary force to achieve this high C_T/C_N ratio. Considering these constraints, the approximation of the C_T/C_N ratio at 0.5 for *T. foetus* was reasonable. While the C_T/C_N ratio can be easily approximated, following the approach used in reference (13), the magnitudes of C_N and C_T were determined based on a minimization of the normal mean-squared error in the instantaneous velocity in x and y (E_x and E_y) between the experimental trajectory, and the model derived trajectory of the cell in the body-aligned frame. Using this optimization method, it was possible to determine C_N and C_T for both linear swimming and turning, as shown in **Table 1.2**. The optimized C_N and C_T values were within the range of values typically reported for flagellated microorganisms, 1.226-2.46 pN·s/um^2 (13, 63, 66-68). Using the optimized values of C_N and C_T, trajectories generated by the model in the body-aligned frame were compared to the experimental trajectories. Based on the comparison of the trajectories in the body-aligned frame, it can be seen that with the optimized values of C_N and C_T, the magnitude and direction of the

vectors from each time point closely match the model trajectory (**Fig. 1.5A&D**). In early attempts at modeling linear swimming, the model trajectories showed similar trends in the direction of vectors, however, the magnitude of the vectors was reduced. This problem was not encountered in the analysis of turning. The reduced magnitude of the initial vectors for linear swimming and the fluid dynamics associated with this reduction are extensively addressed in the **Discussion**.

The ability of the model-derived body-aligned frame trajectories to follow the experimental trajectories, within a tolerable error, validates the C_N and C_T magnitudes identified by the model. However, when considering the angular component of the trajectories that are required to translate the body-aligned frame into the lab frame (defined as the actual trajectory of the cell), the values of C_N and C_T identified by the model have a reduced angular velocity. In (13), a correction factor, α, was applied to increase the magnitude of C_N and C_T to provide enough force to correct for the reduced angular velocity. However, in that work, a unicellular mutant of *Chlamydomonas* was modeled, and the correction factor was used to account for the poor swimming ability of the cell, leading to a large boundary effect. In the case of *T. foetus*, these boundary conditions are minimized due to the swimming ability of this cell. Instead, the correction factor, α, is applied directly to the net moment (**Materials and Methods**) to provide the necessary increase in angular velocity. In terms of the fluid dynamics of the system, the application of α to the net moment means that the forces generated by the flagella are correct, as demonstrated with the body-aligned frame comparison; however, how these forces influence the rotation of the body cannot be accurately described without a correction factor. Considering the complex fluid dynamics at the interface between the cell body and flagella, it was not surprising that a correction factor was necessary to account for the actual rotation of the cell body. It should

Table 1.2. Results from Modeling AnalysisDuring Recovery Stroke

	Linear	Turning
Propulsive Force (pN) **-Free** **-Stalked 1** **-Stalked 2** **-Recurrent** **Total**	 2.91 6.62 4.11 7.05 20.69	 4.86 6.53 6.34 8.37 26.09
C_N (pN•s/µm^2)	1.85×10^{-3}	1.75×10^{-3}
C_T (pN•s/µm^2)	0.93×10^{-3}	0.88×10^{-3}
α	2.76	5.94
E_{Vx}	0.48	0.16
E_{Vy}	0.39	0.43
E_R	0.42	0.49
Flexural Rigidity (N•m^2)	1.55×10^{-21}	

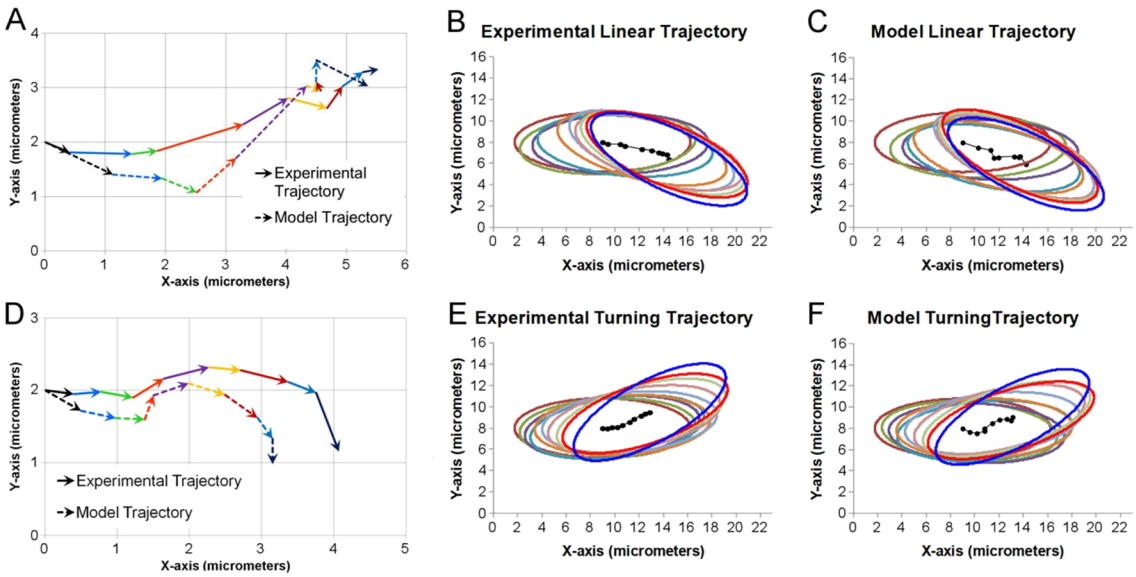

Fig. 1.5 Experimental and model-derived trajectories for linear swimming and turning in both the body-aligned frame and laboratory frame. A) Comparison of the experimental and optimized model-derived trajectories for linear swimming in the body-aligned frame. The vectors from each time point are shown as a different color throughout the course of the stroke. The shape of the trajectories are similar and the trajectories end at similar points. B) Experimental trajectory of an average cell displaying the linear swimming pattern with its flagella. Ellipses have been superimposed around the center of mass to indicate the angular change of the cell. All cells start at the same position and travel in the positive x direction. Despite variations around a central line, the cell proceeds along a linear path with minimal angular changes from the starting and ending points. C) Model trajectory in the laboratory frame using the flagella input from the average linear swimming flagella traces. D) Comparison of the experimental and optimized model-derived trajectories for turning in the body-aligned frame. Note that there is a slight reduction in the x component of the trajectory, with an increased y component. E) Experimental trajectory of an average cell using the turning beating pattern. During turning, the cell has reduced motion in the forward (positive x) direction and has a large angular change of ~30° from its starting orientation. F) Model trajectory in the laboratory frame using the flagella input from the average turning flagella traces. Note that over the course of each stroke the cell follows the same trajectories and angular changes as the experimental trajectories.

be noted that the normal mean-squared error for angular velocity (E_R) before correction was 0.73 for turning and 0.56 for linear swimming. In essence, this low error demonstrates that the instantaneous angular velocity generated from the flagella created the correct angular changes, but with a reduced magnitude. When α was applied to correct for the low angular velocity, the error was reduced to 0.47 for turning and 0.41 for linear swimming. Comparisons of the model-derived and experimental trajectories in the lab frame of reference are shown in **Fig. 1.5B&C** and **E&F**. At the start of each simulation, the cells were oriented the same as **Fig. 1.2A&C**, with the undulating membrane at the bottom of the cell. After validating the model, in terms of both instantaneous angular and linear velocities, as well as the ability to maintain a similar trajectory to the average experimental cells, the model was used to analyze the thrust generated by the flagella during each motion.

Analysis of multi-flagellated propulsion

One of the key contributions from the implementation of the proposed RFT model was the ability to determine the thrust generated by each flagellum. During linear swimming, 20.69 pN of thrust was generated by all of the flagella. The anterior flagella were responsible for 87% of the thrust in the forward direction (along the x-axis of the body-fixed frame), with the recurrent flagella contributing 70% of the thrust along the y-axis in the body-fixed frame. Cumulatively, the free flagellum provides the smallest amount of total thrust, as it is only involved in the first three time intervals, while stalked 1 and the recurrent flagella generate similar thrust values (**Table 1.2**). In addition to the thrust generated by each flagellum, the timing or phase of beating was shown to have a significant effect on propulsion. As shown in **Fig. 1.6A**, during the first 56 ms the free flagellum provides the majority of the thrust, followed by stalked 1 over the next 84 ms, and finally the thrust over the last 112 ms is split between the recurrent flagella and stalked

2. Thus, for linear swimming, propulsion is generated through a highly coordinated beating of each of the anterior flagella over a distinct time interval.

Similar to the analysis of thrust generation for linear swimming, the thrust generated by each flagella during turning was highly coordinated. Over the first 56 ms, the free flagella generated the majority of the thrust; however, unlike linear swimming, the rest of the beat had similar thrust values for both stalked 1 and stalked 2. Considering that these two flagella have a similar beat and orientation during turning, this result was not surprising. Another distinction between linear swimming and turning was the contribution of the recurrent flagella throughout the entire beat motion during turning (**Fig. 1.6B**). Although both strokes appear to have cyclic or periodic contributions from the recurrent flagellum, the thrust generated during turning is much more consistent in magnitude (0.56-1.46 pN) when compared to linear swimming which covers a broader range of thrust values (0.13-2.39 pN). In general, the thrust generated during turning is larger, 26.09 pN, than linear swimming. In fact, only stalked 1 has a similar value for both strokes, 6.61 and 6.53 pN (**Table 1.2**). The ability to predict the thrust generated from multi-flagellar beating not only allows comparison of propulsion between linear swimming and turning in *T. foetus*, but also allows for comparison of propulsion across a wide range of microorganisms employing various swimming strategies.

Discussion

In this work, we combined high-speed high-contrast video microscopy, nanoindentation, and a RFT model to analyze multi-flagellated propulsion using *T. foetus* as a test case. Significant insight into the motion of *T. foetus*, beating characteristics of its flagella, and thrust generation were elucidated. Further, the resulting changes in the fluid dynamics associated with the "spinning" of the cell body are discussed. Based on these results, we have gained greater insight into the biology of *T. foetus*, and more generally into multi-flagellated propulsion.

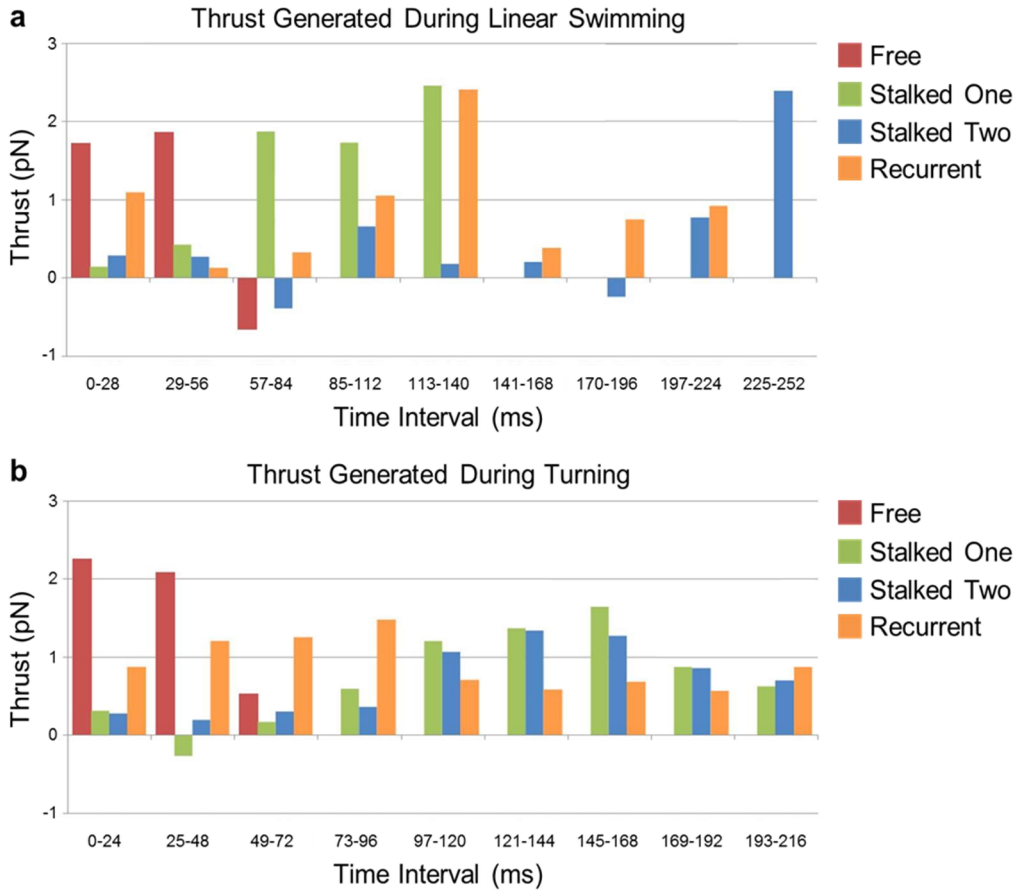

Fig. 1.6 Thrust generated during each time interval of the recovery stroke. A) Thrust generated by each flagellum for linear swimming shows the cyclic nature of this stroke. From 0-56 ms the free flagellum contributed 56% and 69% of the propulsive force. From 57-140 ms, stalked 1 contributed > 50% of the propulsive force. After this interval, the propulsive force was generated by a combination of the recurrent and stalked 2. Over the course of the entire stroke, the recurrent flagellum generated the greatest propulsive force (7.04 pN); however, as mentioned earlier, this force was predominantly along the y-axis. The majority of the forward propulsive force was generated by stalked 1 (6.61 pN). Combined, the total thrust generated from all four flagella during the recovery stroke was 20.69 pN. B) Thrust generated by each flagellum for turning. Similar to linear swimming, over the first 48 ms, the free flagellum provided the majority of the propulsive force (62.5%). For the rest of the stroke; however, stalked 1 and 2 contributed relatively equally to propulsion. This is further confirmed by the total propulsive force generated by stalked 1 and 2 (6.53 and 6.33 pN). The total thrust generated during the course of the turning motion was 26.09 pN, 1.26 times larger than the force generated during linear swimming.

The first major finding of this work was that *T. foetus* was capable of generating two distinct flagellar beating motions to adjust its trajectory from linear swimming to turning. The ability of *T. foetus* to generate multiple waveforms from the same flagellar structure has implications into the underlying biology of the flagella and behavior of the cells. In an effort to further understand potential structural modifications in the flagella of *T. foetus*, and physiological factors that contribute to the change in waveform, examples of other microorganisms capable of generating multiple waveforms are discussed below. One example is the unicellular algae *Chlamydomonas*, which is capable of generating a forward swimming motion through ciliary beating of its flagella, or backward swimming by changing to an undulating waveform (70). Previous studies have demonstrated that the flagella membranes of *Chlamydomonas* play a role in the regulation of calcium to the flagella, which can reversibly alter the flagella motion from ciliary to sinusoidal (70, 71). Further analysis of the central pair microtubules during forward and backward swimming showed that the generation of the different waveforms leads to differential twisting of the central pair with each beat form (72). In *Chlamydomonas* and *Paramecium*, the central pair rotates parallel to the bend plane of the flagella; however, in *Opalina* the central pair rotates perpendicular to the bend plane (72). In general, the twisting of the central pair can occur through modification of the flagella structure, where relaxed flagella have an inherent twist, or through activation of specialized dynein motors that initiate twisting (72). In other microorganisms, such as *T. brucei*, the orientation of the central pair remains fixed throughout beating; however, this organism has a more rigid paraflagellar rod that may prevent free rotation of the central pair (73). Since no paraflagellar rod exists in *T. foetus*, we hypothesize that central pair twisting provides the underlying force for the generation of the two waveforms exhibited by the anterior flagella. Further analysis would be necessary to confirm this hypothesis.

In addition to the structural implications of the multiple flagella waveforms, behaviorally this fine control over direction suggests that the microorganism is responding to environmental cues and adjusting its trajectory to reach a target destination. Similar strategies are used by *E. coli* and *Chlamydomonas*, where the cells change the waveform of their flagella to alter their trajectory in response to a chemical gradient, or photophobic response (74, 75). A recent study on the flagella membrane of *T. foetus* revealed that the anterior flagella have rosettes of integral membrane proteins along their length, which were hypothesized to contribute to active exo- and endocytosis (76). These specialized integral membrane proteins may be involved in active sensing of environmental parameters that provide cues for the cell to change direction. Further, the abundance of these proteins along the length of the anterior flagella may play a key role in controlling local calcium levels, which could initiate the rapid switching between the different flagella waveforms through modification of the central pair, or other unknown mechanisms. In the present study, the cells were grown in a nutrient rich media, preventing analysis of any kind of targeted motion. However, *T. foetus* has shown the ability to invade fetal tissue (77) and to actively adhere to and phagocytose sperm cells (43). It is possible that the highly specialized linear and turning motion evolved as a means to rapidly track and capture its motile prey, sperm.

Associated with the ability of cells to sense environmental changes is the ability of the cell to "search" for desired chemical gradients, and then follow the gradient to reach its target. In bacteria this sort of searching and directed movement is conducted using the well-studied "run and tumble" mechanism (11, 78-81). More recently, "run and tumble" behaviors have been discovered in the eukaryote *Chlamydomonas*, where cells grown in the dark oscillate between nearly straight swimming and abrupt large reorientations in search of nutrients or light (16). Similar "run and tumble" strategies have been hypothesized for *Trypanosoma brucei*, although

this has not been confirmed (82, 83). More recently, a mechanical model was proposed to investigate the potential for "run and tumble" in a migrating amoeboid cell (84). In this work we identified a "run and tumble" type of motion in *T. foetus*, similar to bacteria and *Chlamydomonas*, leading to the hypothesis that *T. foetus* has the ability to sense and track molecular or chemical gradients. While further studies are necessary to validate this hypothesis, this study provides support for the ubiquity of this strategy in microorganisms in general, despite the majority of focus in prokaryotic cells. The discovery of a "run and tumble" mechanism in *T. foetus* has further implications in the treatment of this disease, and if the chemotactic agent(s) can be identified, it may be possible to reduce the pathogenesis associated with this organism.

Another strength of the combined experimental and theoretical modeling approach used in this work was the ability to identify key changes in the fluid dynamics that were not evident from the experimental analysis. While the first iteration of the model for linear swimming generated velocity vectors with similar direction, the magnitude of the vectors was roughly half that of the experimental data. For turning, however, the magnitude and direction of the velocity vectors generated from the model were similar to those measured from experimental trajectories. This suggested that there was a significant difference in the fluid dynamics associated with linear swimming and turning. Considering that the body spins around the longitudinal axis during linear swimming and not turning, it can be hypothesized that there are key changes in the resulting fluid dynamics associated with this type of motion. As noted previously, with the introduction of the correction factor α, current models applying similar methods have been unable to accurately characterize the resulting torque on the cell body at low Reynold's number (13). Considering that the complex fluid dynamics at the interface between the cell body and flagella are still unknown, it is likely that there are significant boundary effects that cannot be

directly accounted for using the current approach. Similarly, in the current work, the fluid dynamics associated with the spinning of the cell body around the longitudinal axis cannot be accounted for. One hypothesis that would explain the reduced magnitude of the velocity vectors predicted by the model for linear swimming is that the spinning of the cell body effectively reduces the drag experienced by the body. While this has not been demonstrated for a prolate ellipsoid at low Reynold's number, recent work has shown that the rotation of other uniquely shaped structures or bodies under similar conditions have increased propulsion efficiency (85, 86). While it was necessary to model *T. foetus* as a prolate ellipsoid, since irregular shapes are too complex, in actuality an undulating membrane wraps around its body from the anterior to posterior region, and it is possible that this structure generates a reduction in drag upon spinning. Further, due to the motion and position of the flagella and undulating membrane during linear swimming in *T. foetus*, it is reasonable to hypothesize that the viscoelastic properties of the localized fluid could be altered as a result of interactions occurring at this interface, as reported for other microorganisms (87). In the work done by Spagnolie et al. (85), it was shown that viscoelasticity can either increase or decrease both the swimming speed and/or swimming efficiency of helical bodies depending on geometry, fluid properties, and rotation rate. Another study regarding the formation of chiral ribbon trajectories of sperm was able to show that the three dimensionality of sperm swimming generates a situation in which the surface area is minimalized, further stating that this could potentially lead to energy minimization corresponding to maximal propulsion efficiency (88). The three dimensionality of linear swimming in *T. foetus* could therefore be a similar strategy in which the spinning of the body creates a minimal surface leading to an increase in propulsion not evident during the turning motion. Although the direct cause and degree to which spinning might affect the propulsion of *T.*

foetus during linear swimming cannot be determined, the results from this study provide additional evidence that this type of rotation could be an efficient strategy for maximizing propulsion at low Reynold's number.

The "spinning" of the cell body around the longitudinal axis also has significant implications on the control of the trajectories. As illustrated in **Fig. 1.1A**, during linear swimming, the 180° rotation of the cell around the longitudinal axis allows the cell to correct for the ~15° change in angle observed for a single recovery stroke. In essence, in the first beat of the linear swimming, the cell will turn ~15° away from the linear trajectory; however, after rotation the second beat, the cell will turn ~15° towards the overall linear trajectory, resulting in a net angle change of 0°. Unlike linear swimming, the lack of "spinning" around the longitudinal axis during turning, as shown by the position of the axostyle in **Fig. 1.2B**, allows the cell to make a sharp angular change or turn, before initiating linear swimming again. Considering the 2D nature of the model and experimental technique, we were not able to conclusively elucidate the structure that provided the initial force to start the cell "spinning." However, based on the differences in the active stroke for turning and linear swimming, we hypothesize that the force for "spinning" is generated by the 3D motion of the active stroke. Further analysis is necessary to analyze this hypothesis.

The final contribution from this work was the ability to analyze the multi-flagellated propulsion of *T. foetus* in the context of other known microorganisms with varying strategies for generating low Reynold's number propulsion. The net propulsive force generated by the flagella in *T. foetus* during the recovery stroke (20-26 pN) was similar to the values obtained for other eukaryotic flagellates. Despite the sinusoidal motion of the flagella in sperm compared to the ciliary beating of the flagella in *Chlamydomonas* and *T. foetus*, the propulsive forces for linear

swimming from all of these organisms fall within a similar range of magnitude, 13.5-25 pN (22, 89, 90). When compared to the propulsive force generated from the rotary flagella of the bacteria *E. coli* and *S. typhimurium*, 0.37-0.57 pN, the eukaryotes have much greater force, although the body size of bacteria is much smaller, thus drag is lower (91, 92). By far the propulsive strategy that generates the most force is the ciliated swimming of *Paramecium*, which generates 7000 pN of force (93). However, *Paramecium* are much larger than the other eukaryotic cells provided for comparison, and the number of cilia is in the thousands. In addition to the overall thrust generated by *T. foetus*, the propulsive force per flagella are within the range of other eukaryotic cells: the flagella of sperm, 6.5-11.1 pN (94), *Chlamydomonas reinhardti*, 2.4 pN (95), and *Volvox carteri*, 0.3-0.8 pN (95). Considering that the total propulsive force generated by the four flagella of *T. foetus* is similar to the force generated by the biflagellate *Chlamydomonas* and uniflagellated sperm, we hypothesize that the multi-flagellated state may have evolved for a separate purpose beyond simple propulsion. A similar hypothesis has been put forward for *E. coli*, where flagellar bundles have been shown to generate similar thrust values compared to individual flagella (96). Similarly, as indicated previously for *Giardia lamblia*, the presence of multiple flagella pairs may aid in precise steering, orientation, and stability (34). For *T. foetus*, a similar trend has been observed, where the recurrent flagella controls angular deviation, while contributing less directly to forward propulsion. Additionally, an increased number of flagella may aid in sensing, attachment, or other key biological functions independent of propulsion.

Materials and Methods

Experimental

T. foetus cultures were purchased from the American Type Culture Collection (ATCC) (strain BP-4 ATCC #30003) and cultured axenically in Diamond's medium. Microscopic analysis was conducted using the CytoViva® (Aetos Technologies, Inc., Auburn, AL) illumination and

imaging system described previously for the analysis of the flagella motion of *Giardia lamblia* (34). Using this system, the flagella motion of *T. foetus* was captured at 167 fps, far superior to previous studies (44, 46). Manual traces of the flagella motion over 10 complete beat cycles were conducted in the ImageJ software package (following inversion of the image colors), and the x-y coordinates of the flagella traces were exported to generate "point clouds" from which the average beat motion was analyzed, similar to the methods outlined in (48). Using the point clouds, it was possible to generate a representation of the flagella motion at 10 different time-points for the recovery strokes. Polynomial fits were used to smooth the average traces and to extrapolate points along the flagella. The polynomials were then used to obtain the velocities of the flagella, and used as the input to the model.

In order to experimentally obtain a value for the Young's modulus of the flagella in *T. foetus*, the cells were fixed with 2.5% gluteraldehyde in Millonig's Buffer and dehydrated using an ascending series of ethanols, prior to air-drying onto coverslips. Nanoscale imaging and nanoindentation of *T. foetus* was performed using an Asylum MFP/3D atomic force microscope (AFM). Cells were first imaged in AC mode using AC240TM cantilevers with a spring constant of 2 N/m and frequency of 70 kHz (**Fig. 1.4A**). After imaging, 1 μm^2 scans were taken on individual flagella (**Fig. 1.4B**). Twenty points were then selected (10 points equally distributed over the coverslip surface and 10 points equally distributed along the center line of the flagellum) and a series of indentations (5 at each point) were performed. A 60 nN trigger force was selected to indent 5 – 10 % into the flagellum to ensure that there were no effects from the underlying glass substrate. This procedure was repeated for 10 different flagella from multiple cells, yielding 1000 total force curves (500 taken on the glass substrate and 500 taken on the

flagella) from which Young's modulus was calculated using the Hertzian model provided in the MFP/3D software.

Modeling

In both linear swimming and turning, the flagella have a planar beating motion, which allows the flagella to be traced. In turning, the lack of rotation of the cell body around the longitudinal axis maintains the planar beat motion of the flagella. During linear swimming, the cell body spins around the longitudinal axis; however, since the flagella are projected in front of the cell, each flagella beats within the plane of the microscopic system during the recovery stroke, allowing for precise flagella tracing. Similarly, only the 2D trajectory of the cell body was determined, since any 3D deviations in trajectory could not be measured. Due to the 2D nature of the microscopic platform, and thus the experimental data, a modified 2D RFT model was implemented to measure the viscous forces on the flagella of *T. foetus* (13). In this 2D model, only rotation of the body in the x-y plane can be accounted for numerically, while spinning of the cell body around the longitudinal axis cannot be accurately represented. The methods and equations shown here follow closely the analysis in reference (13), and are reproduced here for convenience. First, the experimental velocity of the cell body ($\mathbf{v}_G$) was measured using the microscopic platform. In the laboratory frame, the linear and angular velocity of the cell body can be differentiated from the linear and angular displacements of the cell body recorded by the microscopic platform. In order to translate these kinematic variables into forces acting on the cell body, the cell body was transformed to the body-fixed frame with the center of the body as the origin. In the body-fixed frame, the frame translates with velocity, $\mathbf{v}$, and rotates with angular velocity, ω. This is coincident with the body-aligned frame; however, in the body-aligned frame the frame is stationary. To calculate the components of the linear velocity of the cell body, v_x

and v_y, with respect to the body-aligned frame, straightforward transformation of the coordinates was conducted.

The cell body was modeled as a prolate ellipsoid, with a major axis (a), minor axis (b), and eccentricity (e), where $e = \sqrt{(1-\frac{b^2}{a^2})}$. Using this approximation, the viscous drag and torque on the cell body can be calculated from the following equations (13, 97) :

$$F_x = 6\pi\mu avxC_{F1}, \quad [1.1]$$

$$F_y = 6\pi\mu avyC_{F2}, \quad [1.2]$$

$$M_G = 8\pi\mu ab2\omega C_{F3}, \quad [1.3]$$

where

$$C_{F1} = \left(\frac{8}{3}\right)e^3[-2e + \left(1+e^2\right)\ln\left(\frac{1+e}{1-e}\right)]^{-1} \quad [1.4]$$

$$C_{F2} = \left(\frac{16}{3}\right)e^3[2e + \left(3e^2-1\right)\ln\left(\frac{1+e}{1-\mathrm{e}}\right)]^{-1}, \quad [1.5]$$

$$C_{F3} = \left(\frac{4}{3}\right)e^3\left(\frac{2-e^2}{1-e^2}\right)[-2e + \left(1+e^2\right)\ln\left(\frac{1+e}{1-\mathrm{e}}\right)]^{-1} \quad [1.6]$$

and μ is the viscosity of water. Equations 1.1-1.2 govern the viscous drag of the body, while Equation 1.3 shows the relationship between the torque and rotation of a prolate ellipsoid around its minor axis. Equations 1.4-1.6 are the linear drag coefficients of a prolate ellipsoid, and Equation 1f is the drag coefficient of rotation of a prolate ellipsoid around its minor axis [78]. The viscous drag ($\boldsymbol{F_G}$) and net moment ($\boldsymbol{M_G}$) on the body must be balanced by the fluid forces of the flagella ($\boldsymbol{F_f}$ and $\boldsymbol{M_{Gf}}$), as shown below:

$$\boldsymbol{F}_G = \boldsymbol{F}_f, \quad [1.7]$$

$$\boldsymbol{M}_G = \boldsymbol{M}_{Gf}. \quad [1.8]$$

Considering that *T. foetus* has four flagella, the fluid forces and net moment generated from the flagella can be expanded to the following form:

$$\boldsymbol{F}_f = \boldsymbol{F}_{free} + \boldsymbol{F}_{first\ stalked} + \boldsymbol{F}_{second\ stalked} + \boldsymbol{F}_{recurrent} \quad [1.9]$$

$$\boldsymbol{M}_{Gf} = \boldsymbol{M}_{G,free} + \boldsymbol{M}_{G,first\ stalked} + \boldsymbol{M}_{G,second\ stalked} + \boldsymbol{M}_{G,recurrent}, \quad [1.10]$$

To accurately derive the flagellar forces in the laboratory frame, the absolute velocity (lab frame of reference) was calculated from the follow equation:

$$\mathbf{v} = \left(\mathbf{v}\right)_{G_{x'y'}} + \boldsymbol{\omega} \times \mathbf{r}' + \mathbf{v}_{G,} \quad [1.11]$$

where $\left(\mathbf{v}\right)_{G_{x'y'}}$ is the velocity of each point along the flagella in respect to the body-fixed frame, $\mathbf{r}'$ is the position of the flagella element in the body-fixed frame, $\boldsymbol{\omega} \times \mathbf{r}'$ is the velocity due to the rotation of the frame, and $\mathbf{v}_G$ is the velocity of the body in the laboratory frame. Next the velocity was expressed in terms of normal, and tangential coordinates:

$$\mathbf{v} = v_N e_N + v_T e_T \quad [1.12]$$

In Equation 1.12, $\mathbf{e}_N$ is the normal unit vector, v_N is the component of the velocity in the normal direction, $\mathbf{e}_T$ is the tangent unit vector, and v_T is the component of the velocity in the tangential direction. The force of the fluid on an element of the flagella was then calculated using resistive-force theory (13, 61, 65). In RFT, the force/unit length in the normal and tangential direction, f_N and f_T respectively, are attained by multiplying the velocity components in the normal and tangential direction by the drag coefficients C_N and C_T. The drag-velocity equations for the force from the fluid on a particular point on the flagella in the laboratory frame are:

$$f_T = C_T v_T, \quad \text{and} \tag{1.13}$$

$$f_N = C_N v_N. \tag{1.14}$$

It should be noted that the forces exerted by the flagella on the fluid leading to propulsion are equal and opposite to the forces of the fluid on the flagella as described by Equations 1.13 and 1.14. By integrating the force at each point along the length of the flagella, the net force and moment generated by the flagella in respect to the center of mass of the body (F_{xf}, F_{yf}, M_{Gf}) were estimated using the following equations:

$$\mathbf{F}_{flagella,i} = \int_0^{\mathrm{L}} \mathbf{f} \mathrm{ds}, \tag{1.15}$$

$$\mathbf{F}_{flagella,i} = F_{xf,i}\mathbf{e}_x + F_{yf,i}\mathbf{e}_y, \text{ and} \tag{1.16}$$

$$\mathbf{M}_{Gflagella,i} = \int_0^{L} \mathbf{r}' \times \mathbf{f} \mathrm{d}s. \tag{1.17}$$

By using the above net forces and torque, the linear and angular velocities of the cell body were calculated from (13)

$$V_{xf} = \frac{F_{xf}}{6\pi\mu a C_{F1}}, \tag{1.18}$$

$$V_{yf} = \frac{F_{yf}}{6\pi\mu a C_{F2}}, \text{and} \tag{1.19}$$

$$\omega_f = \frac{M_{Gf}}{8\pi\mu a b^2 C_{F3}}. \tag{1.20}$$

The C_T / C_N ratio was then set to the optimum value for a smooth cylinder, 0.5, as described in *Model Validation*. The magnitude of C_N and C_T were estimated using the optimization procedure described in (13). Essentially, the predicted linear velocities of the cell body for each

C_N and C_T value were validated against the experimental trajectories to get the normal mean-squared error in x and y:

$$E_x = \int_0^T \left(v_x - v_{xf}\right)^2 d\tau \,/\, \int_0^T v_x{}^2 d\tau, \qquad [1.21]$$

$$E_y = \int_0^T \left(v_y - v_{yf}\right)^2 d\tau \,/\, \int_0^T v_y{}^2 d\tau, \text{and} \qquad [1.22]$$

$$E = E_x + E_y. \qquad [1.23]$$

The values with the minimum error were chosen for the simulations. To account for the reduced angular velocity a correction factor, α, was applied to the net moment, as shown in Equation 9 and discussed in *Model Validation*.

$$\omega_f = \frac{\alpha M_{Gf}}{8\pi\mu a b^2 C_{F3}} \qquad [1.24]$$

Acknowledgements

This work was supported by the Office of Naval Research Young Investigator Program award (ONR-N00014-11-1-0622 and ONR-N00014-13-1-0667d) under the supervision of Dr. T. McKenna. Mr. Nwandu-Vincent was also supported by the Program for Excellence and Equity in Research, National Institute of Health. The authors are grateful for the support.

Chapter 2
Compare and Contrast leading theoretical analysis techniques used to generate propulsive forces of flagellates

Abstract

The Resistive Force Theory (RFT), and the Regularized Stokeslet Method (RSM) were applied to generate the thrust values of the flagella during locomotion. Then these two theories were compared and contrasted discussing their shortcomings and strongpoints when used in multi-flagellated propulsion. In previous studies, the RSM method has been shown to provide more accurate results (especially in uni-flagellates) due to the fact that it takes into account the flagella-flagella and body-flagella hydrodynamic interactions while the original RFT neglects it. However our results are contrary to the expected outcome; we see the RFT out-performing the RSM in the X and Y directions plus the it led to better angular velocity predictions in both motions. Our results show that the minimization approach we use to calculate the drag coefficients of our model lead to better approximation than the RSM. So with these results we can feel comfortable proceeding with the RFT in 3-D analysis of the *T.foetus* body and flagella kinematics.

Introduction

Johnson and Brokaw(21) compared The Resistive Force Theory to The Slender Body Theory and concluded that even though SBT was more accurate, the RFT was satisfactory for organisms with small cell bodies. Their study was on a uni-flagellate cell and this sort of comparison would greatly aid the field of multi-flagellated propulsion because the cell body-flagella and flagella-flagella hydrodynamic effects are more pronounced in this case.

The equations that governs propulsion in near zero Reynolds number flows is called the Stokes equation,

$$\mu\nabla^2\boldsymbol{u} - \nabla p = \boldsymbol{f}, \text{and} \nabla\cdot\boldsymbol{u} = 0, \qquad [2.1]$$

Where μ, $\boldsymbol{u}$, p, and $\boldsymbol{f}$ are the kinematic viscosity, velocity, pressure and force per unit volume

respectively. Hancock introduced a fundamental solution to this equation called the stokeslet which corresponded to a concentrated point force(18). The stokeslet equation is,

$$\frac{r_0^2\mathbf{f}(s)+\left[\mathbf{f}(s)\cdot\mathbf{r}_0\right]\mathbf{r}_0}{8\pi\mu r_0^3} \qquad [2.2]$$

s is the position of the stokeslet, $\mathbf{r}_o$ is the distance between the stokeslet and the point of interest and r_o is the magnitude of the vector $\mathbf{r}_o$.

The SBT method developed by Lighthill(20) uses a combination of stokeslets and dipoles along the centerline to represent a flagellum. As dipoles strengths decay faster than stokeslets, Lighthill developed a parameter, q, that governs the distance where dipoles have an effect. q is a length characteristic that is $a \ll q \ll L$ (a= radius). He showed that the results could be made independent of q by using dipoles of strength(20),

$$-\frac{r_0^2\mathbf{f}_n(s_0)}{4\mu}, \qquad [2.3]$$

$\mathbf{f}_n$ is the normal force induced by the dipole at s_o.

So the velocity of the point s_o is

$$\mathbf{u}(s_0)=\frac{\mathbf{f}_n(s_0)}{4\pi\mu}+\int_{r_0>\delta}\frac{r_0^2\mathbf{f}(s)+\left[\mathbf{f}(s)\cdot\mathbf{r}_0\right]\mathbf{r}_0}{8\pi\mu r_0^3}ds \qquad [2.4]$$

$\delta=\frac{1}{2}a\sqrt{e}=0.82a$ and is described as the natural cutoff(20). Equation 15 sums up the contribution of the stokeslets along the flagellum and the dipole at s_o to calculate the velocity at s_o

The RFT(20, 61) just takes into consideration the near field component of the SBT and disregards the long range effects of the stokeslets. It replaces the equation with local drag coefficients,

$$\mathbf{u}(s_0) = \mathbf{f}_t \mathrm{C}_t + \mathbf{f}_n \mathrm{C}_n + \mathbf{f}_b \mathrm{C}_b \qquad [2.5]$$

$$\mathrm{C}_t = \frac{2\pi\mu}{\ln\left(\frac{2q}{a}\right)}, \mathrm{C}_n = \mathrm{C}_b = \frac{4\pi\mu}{\ln\left(\frac{2q}{a}\right) + \frac{1}{2}}$$

Where C_t, C_n, and C_b are the drag coefficient in the tangential, normal and bitangent direction respectively.

The regularized stokeslet method uses smoothed point forces at each stokeslet location to calculate the flow induced by a point on the flagellum(23, 25-27). We use Cortez's(26) approximations of the regularized stokeslet to solve the Stokes equation and get,

$$u_j(\mathbf{r}) = \frac{1}{8\pi\mu} \sum_{n=1}^{N} \sum_{i=1}^{3} \mathrm{S}_{\mathrm{ij}}^{\varepsilon}(\mathbf{r} - \mathbf{r}_n) f_{n,i} A_n \qquad [2.6]$$

Where $\mathrm{A_n}$ are quadrature weights, N is the number of stokeslets and the regularized Green function is

$$\mathrm{S}_{\mathrm{ij}}^{\varepsilon}(\mathbf{r}) = \frac{\delta_{ij}\left(r^2 + 2\varepsilon^2\right) + r_i r_j}{\left(r^2 + \varepsilon^2\right)^{\frac{3}{2}}} \qquad [2.7]$$

The Green function forms a matrix describes as

$$\mathrm{S}_{\mathrm{ij}}^{\varepsilon}(\mathbf{r}) = \begin{bmatrix} \mathrm{S}_{11}^{\varepsilon}(\mathbf{r}) & \mathrm{S}_{12}^{\varepsilon}(\mathbf{r}) & \mathrm{S}_{13}^{\varepsilon}(\mathbf{r}) \\ \mathrm{S}_{21}^{\varepsilon}(\mathbf{r}) & \mathrm{S}_{22}^{\varepsilon}(\mathbf{r}) & \mathrm{S}_{23}^{\varepsilon}(\mathbf{r}) \\ \mathrm{S}_{31}^{\varepsilon}(\mathbf{r}) & \mathrm{S}_{32}^{\varepsilon}(\mathbf{r}) & \mathrm{S}_{33}^{\varepsilon}(\mathbf{r}) \end{bmatrix} \qquad [2.8]$$

Equation 17 in matrix form becomes

$$\begin{bmatrix} u_1 \\ u_2 \\ u_3 \end{bmatrix} = \frac{1}{8\pi\mu} \sum_{n=1}^{N} \begin{pmatrix} \frac{r^2+2\varepsilon^2+r_1r_1}{\left(r^2+\varepsilon^2\right)^{\frac{3}{2}}} & \frac{r_1r_2}{\left(r^2+\varepsilon^2\right)^{\frac{3}{2}}} & \frac{r_1r_3}{\left(r^2+\varepsilon^2\right)^{\frac{3}{2}}} \\ \frac{r_2r_1}{\left(r^2+\varepsilon^2\right)^{\frac{3}{2}}} & \frac{r^2+2\varepsilon^2+r_2r_2}{\left(r^2+\varepsilon^2\right)^{\frac{3}{2}}} & \frac{r_2r_3}{\left(r^2+\varepsilon^2\right)^{\frac{3}{2}}} \\ \frac{r_3r_1}{\left(r^2+\varepsilon^2\right)^{\frac{3}{2}}} & \frac{r_3r_2}{\left(r^2+\varepsilon^2\right)^{\frac{3}{2}}} & \frac{r^2+2\varepsilon^2+r_3r_3}{\left(r^2+\varepsilon^2\right)^{\frac{3}{2}}} \end{pmatrix}_n \begin{bmatrix} f_1 \\ f_2 \\ f_3 \end{bmatrix} \qquad [2.9]$$

ε is a regularization factor.

Results and Discussion

The RSM method was supposed to be more accurate than RFT due to the fact it takes into account the flagella-flagella and body-flagella hydrodynamic interactions while the Original RFT neglects it. However in this study we use a modified RFT model that does not use the standard equations to obtain the drag coefficients (C_N and C_T). But instead use a minimization of error procedure to fit the trajectory thus inherently accounting for the hydrodynamic interactions. In this manner it provides a better approximation than both the original RFT and RSM. In the linear swimming motion the RSM has an error of .57 in the X direction, compared to the lower .467 (**Fig.2.1**). This trend is the same in the Y error value (RFT .432, RSM .59); the angular errors are closer to each other but with RFT(.43) still possessing a smaller value than that of the RSM(.48). The turning follows the same pattern as the linear swimming motion (**Fig.2.2**). So with these results we can feel comfortable proceeding with the RFT in 3-D analysis of the *T.foetus* body and flagella kinematics.

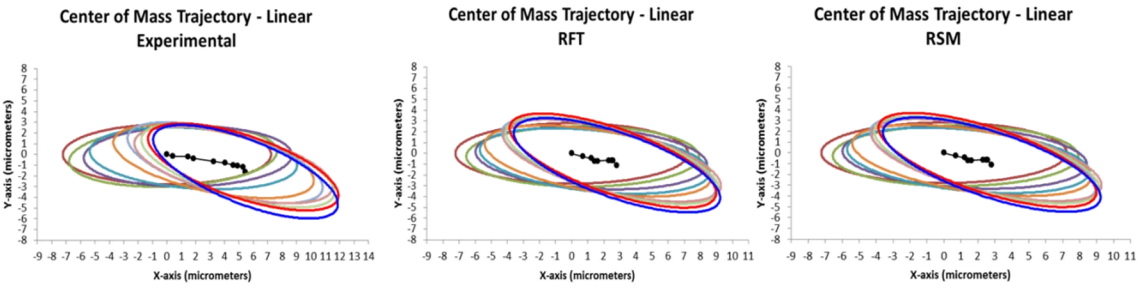

	RFT	RSM
Error in X	.467	.57
Error in Y	.432	.59
α	3.32	2.84
Error in angle	.43	.48

Figure 2.1: Trajectory comparison of Resistive Force Theory and Regularized Stokeslet Method for the linear Trajectory

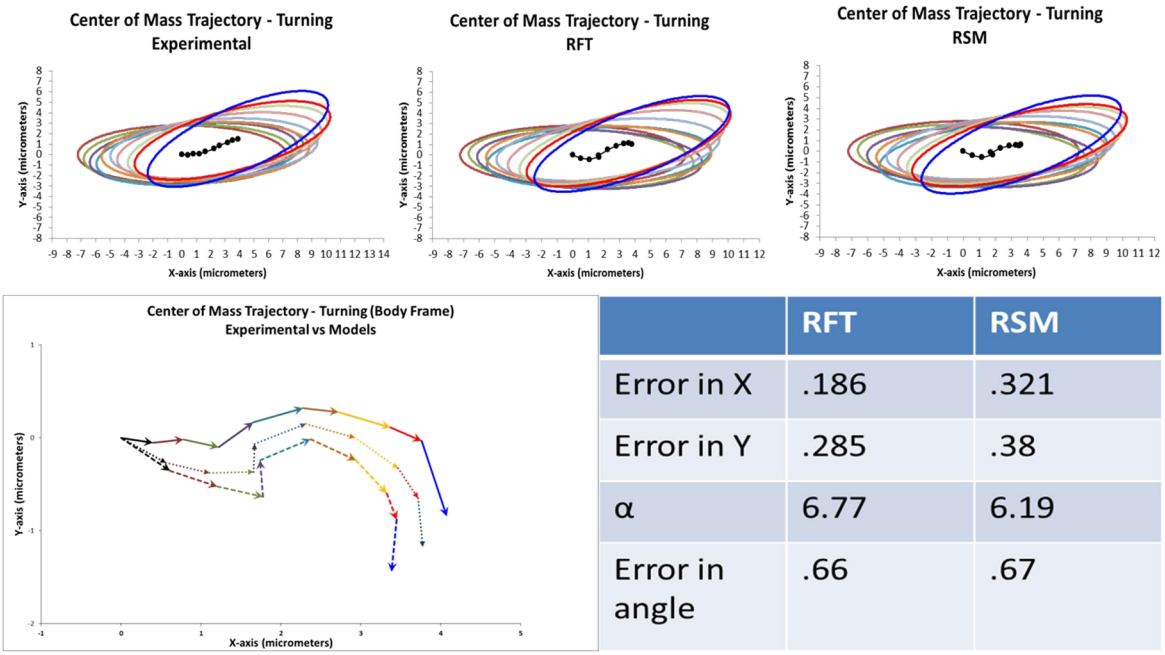

	RFT	RSM
Error in X	.186	.321
Error in Y	.285	.38
α	6.77	6.19
Error in angle	.66	.67

Figure 2.2: Trajectory comparison of Resistive Force Theory and Regularized Stokeslet Method for the turning Trajectory

Chapter 3
Quantitatively Analyze *T.foetus* in 3-D

Abstract

Multi-flagellated propulsion was examined using a high speed 3-D platform and a 3-D resistive force theory (RFT) based model, with the *Tritrichomonas foetus (T.foetus)* serving as a test case. Digital Holographic Microscopy was used to produce the 3-D trajectory of the *T.foetus* for the first time. Also for the first time, a 3D beating pattern of the flagella was generated by finding flagella beat forms that closely matched the cell's trajectory using the mean squared error values as a guide. This allowed for more accurate quantitative measurements and analysis of the forces caused by the flagella and their effect on the body as opposed to the previously acquired 2-D pattern. Along with the body coordinates and flagella beating patterns, this is the first time applying RFT in 3D for a multi-flagellated micro-organism, and with this we were able to further characterize and distinguish between the two distinct beating patterns that produce linear swimming and turning. We find out that the turning mothing dissipates half as much energy(97.95J) as the linear swimming motion (184.73 J) which leads to the belief that the motion is more energy efficient. Also in depth analysis of each flagella's contribution to each dimension was carried out. The energy results coupled with the thrust results show the highly coordinated nature of multi-flagellated propulsion. The low error numbers and similar trajectories produced by this model shows that this method is suitable for analyzing the kinematics of multi-flagellated propulsion.

Introduction

Micro-organisms have developed numerous mechanisms to navigate and maneuver through their low Reynolds number environment; characterized by the inertia forces being greatly overcome by viscous forces. These strategies involve non reversible repeated deformations of body shapes(98) such as the use of flagella and cilia(99); which are thin organelles that propel the cell due to their active bending. The bending and rotation of these organelles results in fluid

displacement and cell propulsion. In prokaryotes, the flagella is driven by a rotary motor which results in the propulsion of the cell(7). While in eukaryotes, the flagella generate motion by the sliding of its microtubules along its length(7, 8, 100). The mechanism that results in flagella and ciliary beat pattern in eukaryotes is still an open question with certain papers hypothesizing that mechanical feedback plays a dominant role in it(101, 102). In order to fully understand this process the forces generated by dynein arms would be needed; direct measurement of flagellar forces would be ideal for this purpose but as this is extremely difficult, estimation of these forces through low Reynolds number fluid mechanic equations would be necessary.

Numerous studies have been done on the hydrodynamics of these organelles(13, 20, 21, 61, 103) but they have mostly been in the case of a uni-flagellated cell. In comparison, little work has been done to understand the hydrodynamic properties of multi-flagellated swimmers. A recent study implemented the Resistive Force Theory (RFT) as the basis of a hydrodynamic model of multi-flagellated nanorobots(104) but scarce studies have been done on the actual multi-flagellated cells that are the inspiration for these robots. In a recent study we applied the RFT(105) to the multi-flagellated *Tritrichomonas foetus* (*T.foetus*) and showed that the RFT was suitable for the multi-flagellated cell propulsion studies. That study as with all others prior were conducted using two dimensional data which leaves out vital components of these organelles motion and resultant effects on both the surrounding fluid and the cell body they are attached to. In this study we remedy this problem by implementing Digital Holography to, for the first time, analyze the three dimensional trajectory of *T.foetus* and analyze its hydrodynamic and kinematic properties using RFT. In our previous work, we have developed a high speed imaging system to qualitatively analyze the propulsion of the octo-flagellated *Giardia lamblia*(35, 106), and then combined this platform with RFT to provide insights into multi-flagellated propulsion through

our quantitative analysis of *T. foetus's* swimming(105). In this work we for the first time use RFT to analyze a multiflagellated cell in three dimensions to extend our analyses and knowledge of multi-flagellated propulsion.

The Resistive Force Theory developed by Gray and Hancock(61), articulates the propulsive force/unit length of the flagellum into normal and tangential components. The forces are attained by multiplying the normal and tangential velocities by normal and tangential coefficients respectively. In our previous work we demonstrated that this technique is suitable for replicating and analyzing the trajectory of multi-flagellated cells(105). In this study we use *T.foetus* as a test case to implement RFT in three dimensions. *T.foetus* is a multi-flagellated micro-organism found in the urogenital tract of cattle and the etiological agent of bovine trichomoniasis. Trichiomoniasis in cattle typically causes vaginitis, abortion, and infertility in cattle and the financial burden associated with the diagnosis and treatment of this pathogen is significant(28-31). *T.foetus* is a lethal pathogen; its ability to maneuver within the body in very treacherous environments is vital to its pathogenesis, which is not thoroughly understood. The *T.foetus* is ideally suited for the study of multi-flagellated propulsion due to the fact all the propulsive forces required from swimming is produced by its flagella. We examine how these cells are able to navigate their environments using well-coordinated multi-flagella configurations; primarily calculating the forces produced by the flagella and how they affect the body. This work will aid in understanding general principles of multi-flagellated propulsion and insights from this study will serve as inspiration for medical bio-robot designs; due to the fact that the bio-robots would be of similar size and will have to navigate similar environments as the microorganism. Our previous work uncovered that the *T.foetus* employs two different anterior flagella beat patterns during its swimming that result in different motions of the cell, similar to the "run and tumble"

phenomenon in petrichous bacteria(10-12) and *Chlamydomonas*(16). This paper will for the first time, obtain a 3D trajectory of the body of *T.foetus,* obtain suitable 3D anterior flagella beating patterns using a novel method, and for the first time implement an RFT model in 3D to quantitatively analyze the cell's propulsion. Through this set up we are able to calculate the thrust generated by the *t.foetus* during its swimming cycle more accurately, calculate the energy dissipation by each flagella and serve as a platform for the further three dimensional analysis of multi-flagellated organisms.

Methods and Materials

Cell Culture and Observation

T. foetus cultures (American Type Culture Collection (ATCC) strain BP-4 ATCC #30003) were provided by another researcher and cultured axenically in Diamond's medium. Analysis of *T.foetus* body motion was analyzed using Lyncee Tec Transmission DHM-T1000 Transmission Digital Holography Microscope. Instead of capturing just intensity images, DHM captures holograms. From this hologram, an image of the intensity and phase are digitally reconstructed. This machine uses the off-axis method to produce holograms. Two coherent beams with a small angle between them are allowed to interfere and produce a hologram.

Body Position Data

The body position was attained by a matlab code that sorted through each z slice of the cell and detected what slice was most in focus using a code found in the work of Pertuz et al.(107). These image "slices" were stored along with the 3D location of its centroid. The xyz distances of the endpoints from the center were obtained, with the z being the height value at that point of the phase image, and this formed the major axis of the ellipse. The angular velocities of the cells were obtained by rotating each major axis to match the major axis of the subsequent time point using Euler angles as shown in Figure 3.1.

These euler angles were then converted to angular velocities with respect to the x,y,z coordinates of the body using the below equation (based on the angles in Figure 3.1).

$$\omega_x = \dot{\phi} sin\theta sin\psi + \dot{\theta} cos\psi \quad [3.1]$$

$$\omega_y = \dot{\phi} sin\theta cos\psi - \dot{\theta} sin\psi \quad [3.2]$$

$$\omega_z = \dot{\phi} cos\theta + \dot{\psi} \quad [3.3]$$

Flagella Traces

The Three dimensional flagella traces (Anterior Flagella) were obtained from average traces of the flagella beating pattern of *T.foetus.* The averages were obtained by observing the cell under the Cytoviva™ microscope and extracting the flagella coordinates(105). From these 2D observation and traces used in our previous work(105), it was recognized that the anterior flagella beat patterns were similar with apparent differences due to the starting orientation and time of beating. We obtained a representative flagella beat pattern of the flagella most in plane then proceeded to 3D rotate the flagella to match the other two average starting positions. We then matched the trajectory of the body derived from the DHM with these average traces by picking appropriate points in their beat patterns that closely produced velocities that matched those acquired for that of the body(Figure 3.2).

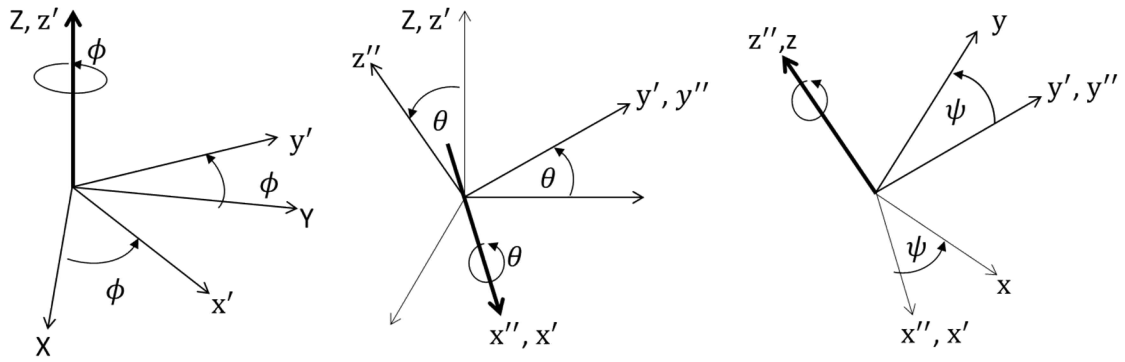

Figure 3.1: Example of rotation using Euler angles. The first rotation is ϕ around the z axis transforming from the initial X,Y,Z system to the x', y', z' system, followed by a rotation of $\boldsymbol{\theta}$ around the new x' axis into the x'', y'', z'' system , and finally a rotation of ψ around the z'' into the x,y,z system.

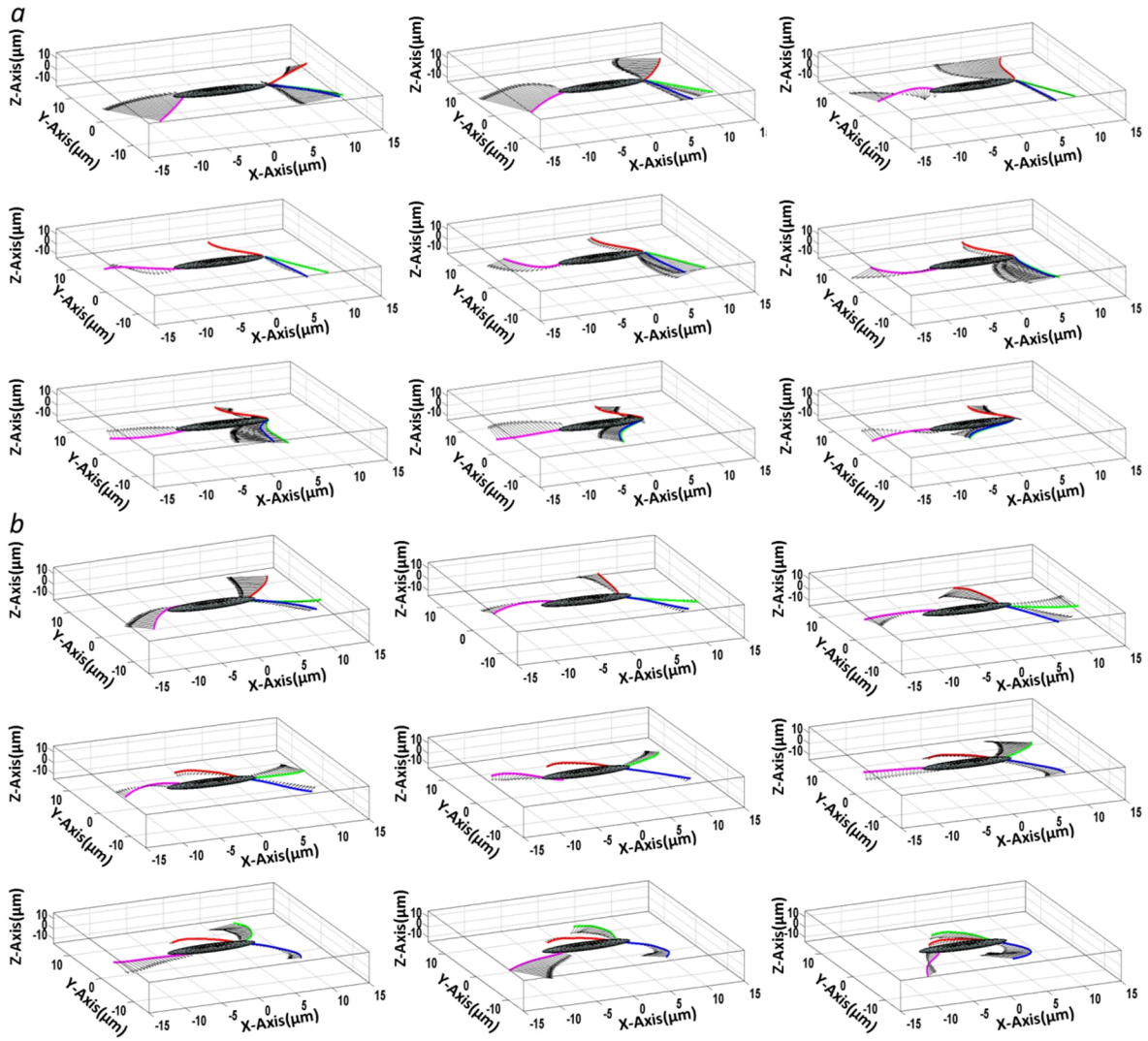

Figure 3.2: The positions of the flagella during both turning and linear swimming with the flagellum force vectors indicated. (a) flagella positions during the turning motion, the figure clearly shows the two stalked flagella beating simultaneously during turning, with force vectors of similar orientation and magnitude. (b) flagella positions during the linear swimming motion, in this motion the stalked flagella beat markedly different from each other. In all images, red indicates the free flagellum, green represents the first stalked flagellum, blue represents the second stalked flagellum, and pink represent the recurrent flagellum.

Resistive Force Model

Modeling

In order to measure the viscous forces on the flagella of *T. foetus*, a modified RFT model was implemented (13). First, the experimental velocity of the cell body ($\mathbf{v}_G$) was measured using the microscopic platform. Next, the cell body was transformed to the body-fixed frame, $V_{x'}$ and $V_{y'}$, to measure the velocities of the flagella. The cell body is modeled as a prolate ellipsoid, with major axis (a) and minor axis (b) and eccentricity (e) where $e = \sqrt{(1 - \frac{b^2}{a^2})}$. The viscous drag and torque on the cell body was then calculated using the below equations (13, 108) :

$$F_x = 6\pi\mu avxC_{F1}, \quad [3.4]$$

$$F_y = 6\pi\mu avyC_{F2}, \quad [3.5]$$

$$F_z = 6\pi\mu avzC_{F2}, \quad [3.6]$$

$$M_G = 8\pi\mu ab2\omega C_{F3}, \quad [3.7]$$

where

$$C_{F1} = \left(\frac{8}{3}\right)e^3[-2e + \left(1 + e^2\right)\ln\left(\frac{1+e}{1-e}\right)]^{-1} \quad [3.8]$$

$$C_{F2} = \left(\frac{16}{3}\right)e^3[2e + \left(3e^2 - 1\right)\ln\left(\frac{1+e}{1-\mathrm{e}}\right)]^{-1}, \quad [3.9]$$

$$C_{F3} = \left(\frac{4}{3}\right)e^3\left(\frac{2-e^2}{1-e^2}\right)[-2e + \left(1 + e^2\right)\ln\left(\frac{1+e}{1-\mathrm{e}}\right)]^{-1} \quad [3.10]$$

and μ represents the viscosity of water. The first set of equations(equations 3.4-3.6) represent the viscous drag on the body while 3.7 shows the relationship between the torque and rotation of the body. Equations 3.8-3.10 are the linear drag equations of a prolate ellipsoid, Eq. 3.8 represents the linear drag in the major axis direction and Eq. 3.9 represents that in both minor axis's direction. With equation 3.10 representing the rotational drag coefficients of a prolate spheroid which is rotating around its minor axis.

By principle, the fluid forces of the flagella must balance that of the viscous drag on the body:

$$\boldsymbol{F}_G = \boldsymbol{F}_f\,, \qquad [3.11]$$

$$\boldsymbol{M}_G = \boldsymbol{M}_{Gf}\,. \qquad [3.12]$$

Since the *T. foetus* has four flagella, the above equation can be expanded to:

$$\boldsymbol{F}_f = \boldsymbol{F}_{free} + \boldsymbol{F}_{first\ stalked} + \boldsymbol{F}_{second\ stalked} + \boldsymbol{F}_{recurrent} \qquad [3.13]$$

$$\boldsymbol{M}_{Gf} = \boldsymbol{M}_{G,free} + \boldsymbol{M}_{G,first\ stalked} + \boldsymbol{M}_{G,second\ stalked} + \boldsymbol{M}_{G,recurrent}\,, \qquad [3.14]$$

In order to obtain precise flagellar forces in the laboratory frame, the global velocity needed to be attained using the below equation:

$$\mathbf{v} = \left(\mathbf{v}\right)_{G_{x'y'}} + \boldsymbol{\omega} \times \mathbf{r}' + \mathbf{v}_{G,} \qquad [3.15]$$

where $\left(\mathbf{v}\right)_{G_{x'y'}}$ is the body fixed frame velocity, $\boldsymbol{\omega} \times \mathbf{r}'$ is the velocity as a result of the rotation of the frame, and the velocity of the body in the laboratory frame is $\mathbf{v}_G$**.** $\boldsymbol{\omega} \times \mathbf{r}'$ and $\mathbf{v}_G$ were added to the body fixed frame velocity depending on the direction of the velocity of the body in respect to the flagella. Next the velocity was expressed in terms of normal, tangential and binormal coordinates:

$$\mathbf{v} = v_N \mathbf{e}_N + v_T \mathbf{e}_T + v_B \mathbf{e}_B. \qquad [3.16]$$

The force of the fluid on an element of the flagella was then calculated using resistive-force theory (13, 61, 65). The theory articulates the force/unit length in the normal, tangential and binormal direction, f_N, f_T and f_B respectively. f_N, f_T *and* f_B are attained by multiplying the velocity components in the normal, tangential and bitangent direction by the drag coefficients C_N, C_T, and C_B.. The drag-velocity equations for the force from the fluid on a particular point on the flagella is:

$$f_T = C_T v_T, \quad [3.17]$$

$$f_B = C_B V_B, \text{ and} \quad [3.18]$$

$$f_N = C_N v_N. \quad [3.19]$$

The net force and moment in respect to the center of the body ($F_{xf}, F_{yf}, F_{zf}, M_f$) were calculated by integrating the force at each point along the length of the flagella using the follow equations:

$$\mathbf{F}_{flagella,i} = \int_0^L \mathbf{f} ds, \quad [3.20]$$

$$\mathbf{F}_{flagella,i} = F_{xf,i}\mathbf{e}_x + F_{yf,i}\mathbf{e}_y + F_{zf,i}\mathbf{e}_z, \text{ and} \quad [3.21]$$

the moment applied to the center of the body being calculated by cross multiplying the position of the flagella by its body frame force.

$$\mathbf{M}_{Gflagella,i} = \int_0^L \mathbf{r}' \times \mathbf{f} ds.. \quad [3.22]$$

Then the linear and angular velocities of the cell body were calculated from (13)

$$V_{xf} = \frac{F_{xf}}{6\pi\mu a C_{F1}}, \quad [3.23]$$

$$V_{yf} = \frac{F_{yf}}{6\pi\mu a C_{F2}}, \quad [3.24]$$

$$V_{zf} = \frac{F_{zf}}{6\pi\mu a C_{F2}}, \text{ and} \quad [3.25]$$

$$\omega_f = \frac{M_{Gf}}{8\pi\mu a b^2 C_{F3}}. \quad [3.26]$$

In the 3D case, $\boldsymbol{\omega}_f = (\omega_x, \omega_y, \omega_z)$. The C_N and C_T were obtained from our previous work on the *T.foetus*(105) and we set $C_B = C_T$. We validated our predicted linear velocities of the cell body against the experimental trajectories by calculating the normal mean-squared error in x, y and z:

$$E_x = \int_0^T \left(v_x - v_{xf}\right)^2 d\tau \Big/ \int_0^T {v_x}^2 d\tau, \quad [3.27]$$

$$E_y = \int_0^T \left(v_y - v_{yf}\right)^2 d\tau \,/\, \int_0^T v_y{}^2 d\tau, \qquad [3.28]$$

$$E_z = \int_0^T \left(v_z - v_{zf}\right)^2 d\tau \,/\, \int_0^T v_z{}^2 d\tau, \text{ and} \qquad [3.29]$$

$$E = E_x + E_y + E_z\,. \qquad [3.30]$$

A correction factor, α, was applied to the net moment to account for the reduced angular velocity.

$$\omega_f = \frac{\alpha M_f}{8\pi\mu a b^2 C_{F3}}\,. \qquad [3.21]$$

Along with force calculations, we also calculated the energy dissipated by each point along the flagella during swimming,

$$ED = \int_0^t \mathbf{F}_{flagella,i} \cdot \mathbf{V}_{flagella,i} dt \qquad [3.22]$$

ED is the Energy dissipated per length of that point on the flagella. *ED* was then integrated along the length of the flagella to get the total Energy dissipated.

Computational Approach

For this work, extensive computational work was done to reach our goal. The following is a step by step process of the procedure used to get the kinematic data of the cell from DHM images

1. Images from the DHM were analyzed at different z-slices. As explained earlier a code found in the work of Pertuz et al.(107) was used to analyze each z-slice to find the slice with the most focus of the cell.
2. The height (z position) of this slice is stored and then an image processing code is used to find and store the x and y center of the cell.

3. The above two steps are done at consecutive time points. The difference between body positions result in linear and angular velocities.
4. These velocities then serve as the experimental body frame velocity in equation 3.15
5. 2-D flagella traces serve as the second set of inputs into the RFT model.
6. The model is run for the first time interval. If results fall within tolerable error in respect to the actual experimental trajectory, we move on to the next time interval.
7. If the model produces unfavorable results, the flagella traces are then 3-D rotated with the goal of cutting down the error.
8. The new rotated flagella traces are then put back into the model. This procedure is repeated until tolerable errors are reached. Then we can proceed to the next time interval.
9. After all the intervals have been satisfied the trajectory of the cell is then produced.

From the trajectory and resultant velocity, the force and energy values can be calculated.

Results and Discussion

T.foetus trophozoites were captured at 1000 fps, approximately 6 times faster than the rate of capture of our previous work(105). Morphologically, the cell is characterized by a spindle shaped body with three flagella extending from the anterior region of the cell, and a recurrent flagellum originating near the anterior, extending towards the posterior with intermittent attachments to the cell body. The intermittent attachment of the recurrent flagella to the cell body leads to the formation of the undulating membrane, which terminates at the posterior region of the cell leaving the free posterior flagellum. After the analysis of more than 100 cells, the two distinct cell body trajectories found previously(105) were confirmed; linear and turning swimming. The three dimensional trajectory of cells swimming using these distinct motions were derived using DHM. Digital Holographic Microscopy has been used in previous work to track the positions of organisms. Sheng et al used it to track dinoflagellates's behavior in the presence

of their prey(109) while Wilson et al applied this imaging technique to analyze the wave form of the microgamete of the malaria parasite(110). The dinoflagellates studied in the former study ranged between 5-20 μm and it was body motions not flagella motion that were tracked. The microgametes on the other hand are flagella and are 200nm in width and about 10 μm in length similar to that of our flagella. But unlike in the case of the *T.foetus* these microgametes are isolated and not attached to a body almost 50 times its width making them easier to track and analyze. This is the first time a combination of the organisms' trajectory and their flagella in relation to it has been studied using DHM. Due to the refractive index of the Trichomonad media and that of the flagella being too close to each other plus the huge body with in relation to the flagella, the DHM was unable to qualitatively capture the flagella motions. So using the method discussed in the Material and Methods session, representative flagella patterns were created. In order to validate these flagella patterns along with the 3D RFT model, a model derived body aligned frame trajectory of these two motions was analyzed and compared with the experimental trajectories (**Figure 3.3**). The model-derived trajectories were able to follow the experimental trajectories within a tolerable error (**Table 3.1**) thus validating the approach. The errors that were calculated, especially those of the angular velocity, could be a result of the recurrent flagellum being modelled with a 2-D beating pattern. Due to the inability to see the flagellum in 3D, the assumption of a 2-D beat pattern had to be made. With the approach being validated, forces of the flagella during the propulsive stroke of the cell could now be calculated and analyzed. Once again due to the lack of knowledge of the flagella beat pattern during its active stroke because of it being obstructed by the body, only the propulsive strokes average flagella beat pattern could be generated.

The major advantage of the proposed RFT model is the capability to derive each's

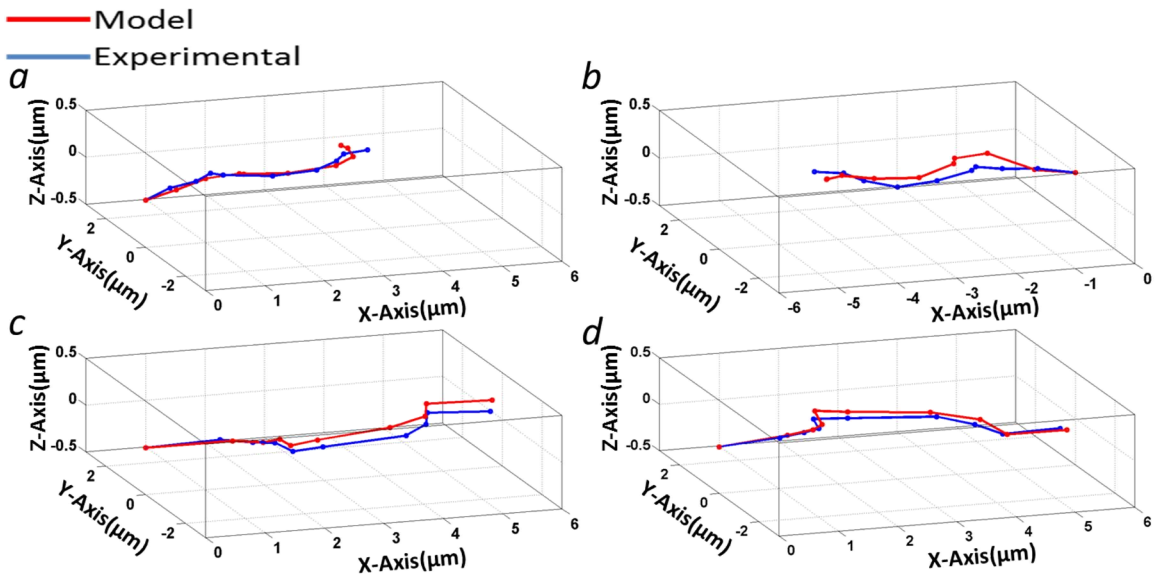

Figure 3.3: Comparison of experimental and model-derived trajectories for turning and linear swimming in both the body-fixed frame and laboratory frame. A) Body- fixed frame comparison of Experimental and model-derived trajectories for turning. The shape and length of the trajectories are similar. B) Lab frame comparison of experimental and model derived trajectory of a cell exhibiting the turning motion pattern with its flagella. C) Body-fixed frame comparison of Experimental and model-derived trajectories for the linear swimming motion. The shape and length of the trajectories are similar. D) Lab frame comparison of experimental and model derived trajectory of a cell exhibiting the linear swimming motion pattern with its flagella.

Table 3.1: Results From Modelling Analysis of Propulsive Stroke

	Turning	Linear
Propulsive Force (pN)		
Free	**14.64**	**8.43**
stalked 1	**17.59**	**12.66**
stalked 2	**18.51**	**7.48**
Recurrent	**29.23**	**13.18**
total propulsive force (pN)	**79.98**	**41.75**
Normalized Energy Dissipation (J)		
Free	**21.13**	**32.85**
stalked 1	**17.75**	**56.59**
stalked 2	**17.49**	**33.73**
Recurrent	**41.59**	**61.56**
Total Energy Dissipation (J)	**97.95**	**184.73**
C_T **(pN s µm^{-2})**	**0.88×10^{-3}**	**0.93×10^{-3}**
C_B **(pN s µm^{-2})**	**0.88×10^{-3}**	**0.93×10^{-3}**
E_X	**.069**	**.021**
E_Y	**.218**	**.079**
E_z	**.061**	**.278**
$E_{\omega x}$	**.437**	**.861**
$E_{\omega y}$	**.380**	**.775**
$E_{\omega z}$	**.530**	**.817**
α	**4**	**1**

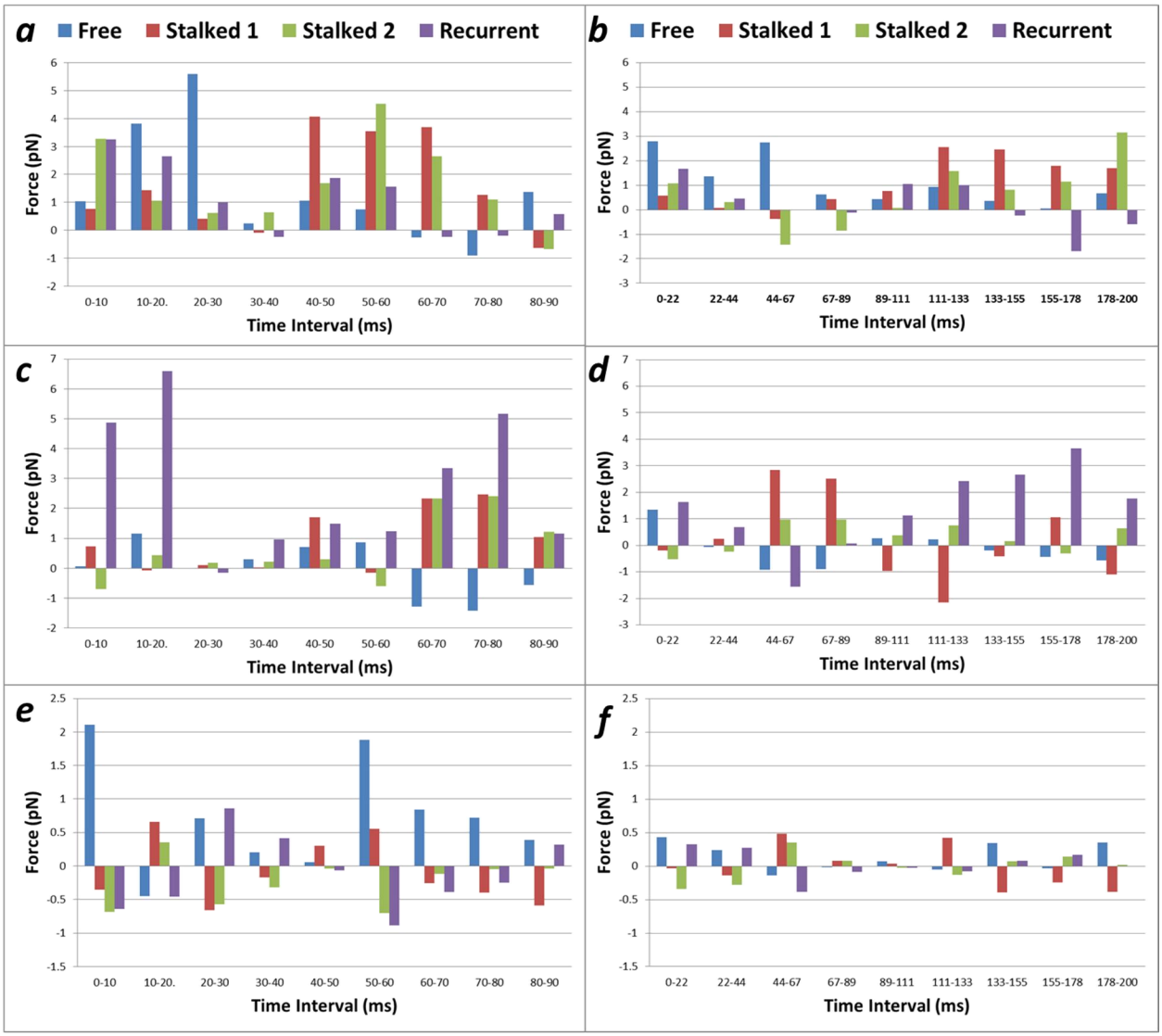

Figure 3.4: Force generated by each flagellum during each time interval of the propulsive stroke. Thrust generated by each flagellum for turning in the a) x-axis c) y-axis e) z-axis shows that the propulsive characteristics of this stroke is cyclical in nature. Also the force generated in the linear motion in the b) x-axis d) y-axis and f) z-axis also show a cyclical pattern with the stalked flagella beating dissimilarly unlike the linear motion.

flagellum's contribution to the propulsion of the cell by determining its thrust (**Figure 3.4**). All four flagella generated a total of 41.75 pN of thrust in the linear swimming motion. The Anterior flagella thrust values showed a similar cyclical characteristic when compared to the values of the 2-D case(105), with the free flagella providing 68% of anterior flagella thrust during the first third of the swimming motion, then the first stalked providing 50% of the anterior flagella thrust for the second third of the motion and finally the second stalked flagella contributing 45% of the anterior flagella thrust during the last third of the motion. When analyzing the force output of the recurrent flagellum, we see that it only is responsible for 6% of the forward thrust (along the x-axis of the body-aligned frame), 22% of the forward thrust of the body in the z-axis but provides 79% of the force in the y-axis of the body-aligned frame. Even though it was modeled as having a planar pattern, the z velocity of the body and its subsequent effect on angular velocity add a z component to the recurrent flagella force. When analyzing the force contributions of the flagella in the x-direction (**Fig.3.4b)** it is clear to see the cyclical nature of the contributions, the free flagellum dominate the force output for the first third of the cycle followed by the first stalked for the next third with the second stalk opposing the forward motion in this direction and then the second stalked for the last third. The recurrent

flagellum produces minimal values and even proceeds to oppose the forward motion for the last third of the cycle. In the y-direction (**Fig.3.4d**), the pattern is less distinguishable. The recurrent flagellum steadily drives the cell forward with each anterior flagella alternating between contributing towards the forward motion or opposing it. In the z-direction (**Fig.3.4f**), the free and recurrent flagella contribute to the forward motion and their forces are slightly greater than that of the stalked flagella whose forces oppose the motion. This analysis shows the highly

coordinated and balancing contributions that each flagella produce towards the movement of the body in this motion.

During the entire course of the swimming motion, the recurrent flagella provided the most total thrust, with the first stalked providing the second most, then the free and then the second stalked (**Table 3.1)**. The anterior flagella force contributions seem to be counter to that which was found in our previous study(105), where the free flagella had the lowest amount of total thrust output. The reason for this discrepancy is that for the previous work, since we could not see the free flagella's beat behind the body, we stopped analyzing its beat pattern. The method used in this work allows for us to predict the flagella's beat even when it would be obstructed by the body as long as the total flagella contribution matched the trajectory of the body. The total thrust output of 41.75 pN seems significantly greater than the thrust output we got for the 2-D case, but this is misleading. The duration of the propulsive beat is different in both cases; .2s in this work compared to .255s in the previous work. When the time is normalize to mimic that of the previous work, the total force output is 32.75pN. This is still greater than the reported 20.69pN of the previous work. The extra force can be attributed to the added z-direction forces and the extended beating duration of the free and first stalked flagella.

In the case of the turning motion, all four flagella generated a total of 79.98 pN. When the duration of the beat was normalized to match that of our previous study, the total thrust output was 32.9pN compared to the previous value of 26.09pN. As in the case of the linear motion, the anterior flagella thrust values trended together with the previously discovered values in the 2-D case(105), the free flagella produces 64% of the anterior flagella thrust for the first third of the motion, but then its contribution significantly reduces to 21%, and by the last third its force contribution is opposite that of the motion of the cell. The free flagella seems to stop during the

second third of the motion and beat very slightly in the opposite direction during the last part of the motion, this backward beating allowed for the model to match the cell's z and angular trajectory. Once again the ability to predict the flagella's beat pattern past the first third enhances our understanding of this motion. The two stalked flagella intuitively exhibit similar thrust values throughout the cycle due to their similar beat form. In this motion the recurrent flagellum opposes the forward thrust in the z-direction, it contributes 20% of the x-axis thrust while contributing 64% of the y-axis thrust. In the x-direction (**Fig. 3.4a**), the free flagella dominate the first third of the force output and the stalked flagella dominate the rest of the motion with the recurrent producing minimal values. In the y-direction (**Fig. 3.4c**), the recurrent flagellum is the major driving force for the forward motion with the anterior flagella contributing significantly less to the forward motion. The free flagellum actually opposes the motion during the last third of the motion. In the z-direction(**Fig. 3.4e**), the free flagellum solely contributes to the forward motion while the other three oppose it. Like for the linear motion the turning motion shows a highly coordinated contribution from each flagella towards the forward movement of the body in all three directions. Cumulatively, the recurrent flagella produced the most thrust during the turning motion, while the free produced the least and the two stalked exhibited similar total thrust values.

The values for thrust from each flagella are in accordance with previous thrust measurements from the flagella of sperm, 6.5-11.1 pN (94), *Chlamydomonas reinhardti*, 2.4 pN (95), and *Volvox carteri*, 0.3-0.8 pN (95) but significantly higher than bacteria (*E. coli* and *typhimurium)* flagella 0.37-0.57 pN which experience significantly less drag due to their smaller body size (92, 111). All the studies cited conducted measurements based on an assumed 2-D model except for that of *typhimurium*, which was calculated directly using a complicated negative

dielectrophoretic method. Converting these 2-D models to 3-D would provide more detailed and accurate kinematic data to properly quantify and contrast flagella behavior and trend. The major area of significance for the extension to 3-D is the ability to accurately track the trajectory of these cells, prior to this data, only planar motions can be analyzed and thus severely limiting knowledge of these organisms. For *T. foetus*, a similar trend to that of *Giardia lamblia*(34) has been observed, where the recurrent flagellum provides stability control and helps regulate angular deviation, but provides only a small contribution to forward propulsion. The fine control over direction indicates that eukaryotes, like *T. foetus* and *Chlamydomonas(75)*, are capable of adjusting their trajectory based on environmental cues similar to the run and tumble characteristic of prokaryotic cells(74).

Using this model we can for the first time compare the Energy dissipated by the flagella during both swimming motions of the cell. We normalized both motions so that they had the same duration so as to be able to correctly compare the energy dissipation difference from the two different motions. This way the only difference between both motions was the flagella beat pattern and nothing else. The turning motion dissipated a total of 97.95J with the recurrent flagellum dissipating the most energy (41.59 J) and the anterior flagella all having relatively similar values. It also exhibited the same time coordinated cyclical characteristic that the thrust values possessed. The linear motion dissipated approximately twice as much energy as the turning (184.73 J) with the recurrent flagellum once again dissipating the most energy (61.56 J). The free flagella and stalked two exhibit similar values at 32.85 J and 33.73 J respectively, but the first stalked flagella this time does not trend with the other two anterior flagella (56.86 J). An intuitive explanation for the difference between the energy dissipation values is that in the linear swimming motion, the flagella cover more distance than in

the turning. This especially obvious when the motion of the first stalked flagella is analyzed; in the turning motion it begins below the body and is pulled towards it while in the straight motion, it begins below the body begins to be pulled (clockwise) towards the body(below) then it beats counterclockwise above the body and then pulled in to the body above. For the linear motion; in the x-direction (**Fig. 3.5b**), the energy dissipation is dominated by the anterior flagella, first by the free then the first stalked and then the second stalked. In the y-direction (**Fig. 3.5d**), the first stalked initially dissipates the most energy then the recurrent dominates the latter part of the motion. The free flagellum and second stalked flagella dissipate relatively insignificant energy when compared to the other two. In the z-direction (**Fig. 3.5f**), the free and first stalked flagella dominate the energy dissipation with the other two dissipating significantly less energy. When the turning motion is analyzed; in the x-direction (**Fig. 3.5a**), the free flagellum dissipates the most energy at the beginning of the motion then the stalked flagella dominate towards the end. In the y-direction (**Fig. 3.5c**), the recurrent flagellum dominates the energy dissipation by far, rendering the energy dissipation from the anterior flagella insignificant. And in the z-direction (**Fig. 3.5e**), the pattern in the y-axis is repeated except that this time it is the free flagellum dissipating the energy and the other three being insignificant. The energy results highlight the difference in beat pattern of the flagella during these two motions; suggesting the possibility of *T.foetus* actively responding to environmental cues and changing its beat pattern due to them similar to the "run and tumble" strategies of bacteria(11, 78, 79, 81) and *Chlamydomonas*(16). The huge energy difference due largely to the change in direction of the first stalked flagella leads to interesting biological implications that would not have been noticed without the implementation of the model. As explained earlier and shown in **Fig. 3.2** the first stalked flagella covers more ground in the linear motion by beating in the opposite direction of its turning

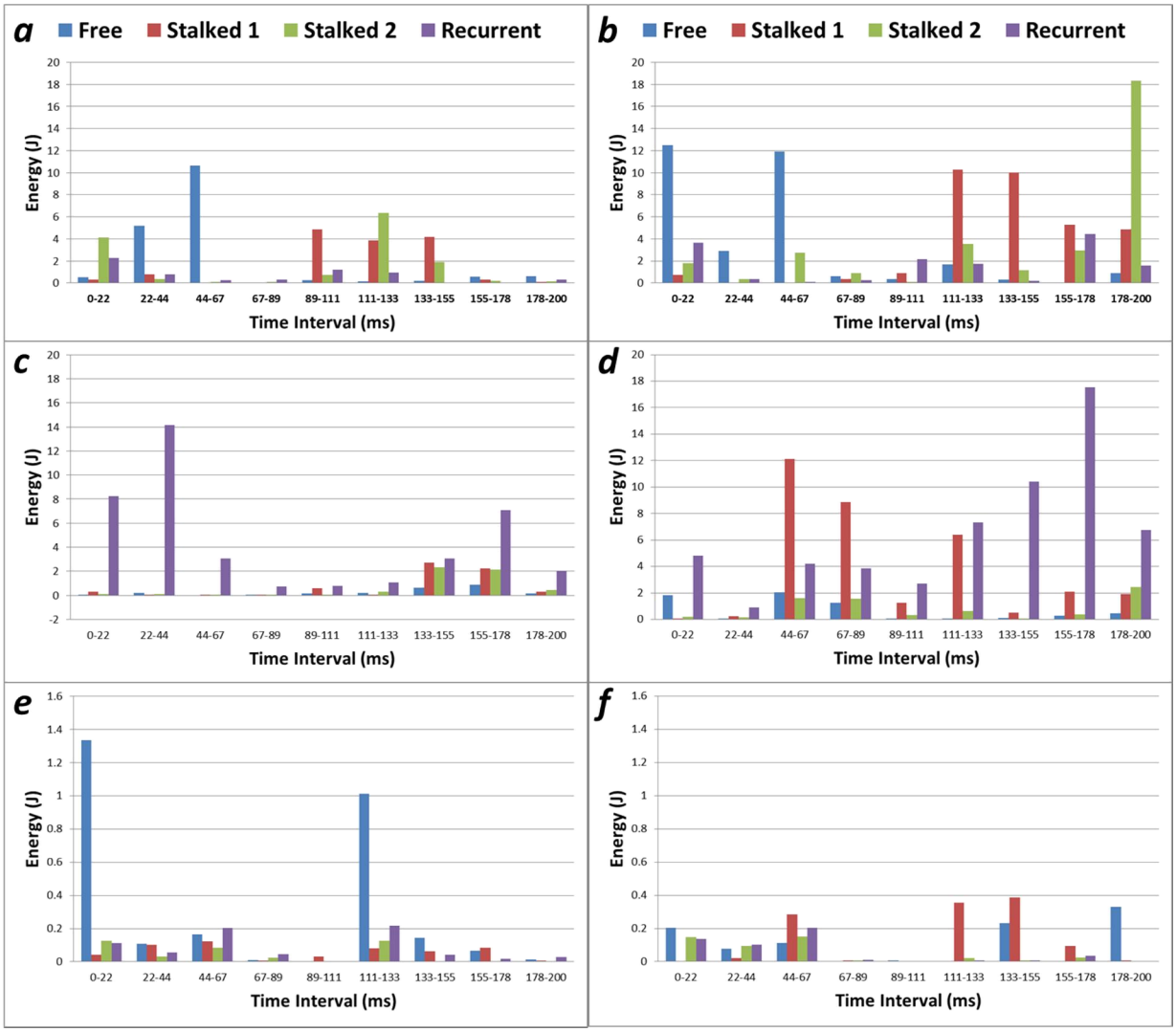

Figure 3.5: Energy Dissipated by each flagellum during each time interval of the propulsive stroke. Energy dissipated by each flagellum for turning in the a) x-axis c) y-axis e) z-axis show the recurrent flagella dominating the energy dissipation in the y-axis while the anterior flagella dominate in the x and z axis. Also the energy dissipated in the linear motion in the b) x-axis d) y-axis and f) z-axis also show a similar pattern but with the values significantly greater

motion. This sort of change in direction leads to the hypothesis that a change in twisting of the central pair microtubules might be responsible for this. It is already known that in *Chlamydomonas* different waveforms led to differential twisting in each beat form (72). This sort of phenomenon could be caused by activation of specialized dynein motors, through calcium gradients or mechanical feedback, that result in central pair twisting (72).

The ability to correctly estimate the thrust and energy dissipation contributions of each flagella leads to very exciting opportunities. First, these forces can be used to correctly derive and analyze the details of dynein activity in the flagella. This would result in better understanding of pathogens and lead to possible treatments for trichomoniasis and other pathogen related maladies. Also understanding the dynein activity could result in treatments for maladies that are caused by disorders of ciliary motions like infertility, respiratory tract infections and congenital defects. Another use for this ability is in the area of bio-robotics. This work will aid in understanding general principles of multi-flagellated propulsion and insights from this study will serve as inspiration for medical bio-robot designs; due to the fact that the bio-robots would be of similar size and will have to navigate similar environments as the microorganism. Due to the robust use of flagella and cilia-like organelles as propulsive structures in swimming microorganisms, the fluid mechanics involved in locomotion of microorganisms has received significant attention for its practical use in micro-robot design (112-114). The possibility of using nanotechnology to manufacture bio-robots to aid in medical applications has led to expectations of immense breakthroughs in patient care. These bio-robots would aid in the diagnosis and treatment of a wide range of ailments from broken limbs to cancer. The bio-robots will be able to navigate the human body to reach previously inaccessible areas to deliver drugs, perform operations or take images(115). Multi-flagellated micro-organisms serve as a better

alternative to the more studied uni-flagellates due to the ability for them to exhibit more control by specializing specific flagella for certain propulsive tasks like we exhibited with the *T.foetus*, recurrent flagellum providing stability control and regulating angular deviation while the anterior flagella contributes to largely to forward propulsion. However, few studies have analyzed the mechanics of flagella in order to understand the actuation pattern along the flagellum and the associated mechanical energy supply and dissipation to the fluid during the swimming. Such information will be the key to understanding the efficiency and mechanics of propulsion by microorganisms, and to further understand biological principles underneath for bio-inspired engineering design. In the present work we have used our integrated model and platform to demonstrate the ability to quantify these mechanical properties and kinematics of flagella in the more accurate three dimensions.

Conclusion

This project was the first time the 3D trajectory of *t.foetus* has been obtained, prior to this study only 2D trajectories of the body of this organism had been obtained, thus study allows for the in-depth study and analysis of the organisms true trajectory. The pathogenesis of this organisms is currently unknown, an in depth and accurate understanding of its propulsion and trajectory towards its host would greatly help in understanding its pathogenesis. Along with the body trajectory, this was the first time a 3D beating pattern of the flagella has been generated, these flagella patterns that match the motion of the body could serve as inspiration for the design of biorobots that would mimic this organism's motion. Also the three dimensionality of the flagella pattern allow for more accurate measurements of forces caused by the flagella and their effect on the body as opposed to the previous 2-D pattern. Energy analysis in all three dimensions was also possible for the first time due to this work.

Along with the body coordinates and flagella beating patterns, this is the first time applying RFT in 3D for a multi-flagellated micro-organism. RFT is usually used for uni-flagellated organisms in 2D, in our previous paper we adapted it for a multi-flagellated organism and now we extend it to the 3D domain. The low error numbers and similar trajectories produced by this model shows that this method is suitable for analyzing the kinematics of multi-flagellated propulsion.

Conclusion and Future Work

Thesis Summary

The work described in this thesis has been concerned with the ability to quantitatively and qualitatively analyze and understand multi-flagellated propulsion. For this purpose, a high-speed high contrast video microscopy, Digital Holography Microscopy, nanoindentation and Resistive Force Theory (RFT) and Regularized Stokeslet Method (RSM) model was combined to analyze multi-flagellated propulsion using *T. foetus* as a test case.

In Chapter 1, multi-flagellated propulsion was comprehensively analyzed using both video microscopy and a RFT model. From the video microscopy analysis, the first major breakthrough of this work was finding that *T. foetus* was capable of generating two distinct flagellar beating motions to adjust its trajectory from linear swimming to turning. The ability of *T. foetus* to generate multiple waveforms from the same flagellar structure has implications into the underlying biology of the flagella and behavior of the cells. The multiple flagella waveforms and resultant fine control over direction suggests that the microorganism is adjusting its trajectory due to its response from environmental cues. This phenomenon is also observed in *E. coli* and *Chlamydomonas*, where the cells change the waveform of their flagella to alter their trajectory in response to a chemical gradient, or photophobic response. *T.foetus* have specialized integral membrane proteins along their lengths and these may be involved in active sensing of environmental parameters that provide cues for the cell to change direction. Further, the abundance of these proteins along the length of the anterior flagella may play a key role in controlling local calcium levels, which could initiate the rapid switching between the different flagella waveforms through modification of the central pair, or other unknown mechanisms. Previous studies have shown that *T. foetus* have the ability to invade fetal tissue (77) and to actively adhere to and phagocytose sperm cells (43); this leads to the possibility that the highly

specialized linear and turning motion evolved as a means to rapidly track and capture its motile prey, sperm.

Related with the ability of cells to change its trajectory due to environmental cues is its ability to "search" for desired chemical gradients, and then follow the gradient to reach its target. In bacteria this sort of searching and directed movement is conducted using the well-studied "run and tumble" mechanism (11, 78-81). More recently, "run and tumble" behaviors have been discovered in the eukaryote *Chlamydomonas*, where cells grown in the dark oscillate between nearly straight swimming and abrupt large reorientations in search of nutrients or light (16). In this work, a "run and tumble" type of motion in *T. foetus* was identified, similar to bacteria and *Chlamydomonas*, leading to the hypothesis that *T. foetus* has the ability to sense and track molecular or chemical gradients. While further studies are necessary to validate this hypothesis, this study provides support for the ubiquity of this strategy in microorganisms in general, despite the majority of focus in prokaryotic cells. The discovery of a "run and tumble" mechanism in *T. foetus* has further implications in the treatment of this disease, and if the chemotactic agent(s) can be identified, it may be possible to reduce the pathogenesis associated with this organism.

By using a combined experimental and theoretical modeling approach it was able to identify key changes in the fluid dynamics that were not evident from the experimental analysis. At first the RFT model when applied in the linear swimming case it resulted in velocity vectors with similar direction as the experimental data, but the magnitude of the vectors was roughly half that of the experimental data. But in the turning case, both the magnitude and direction of the velocity vectors were approximately the same for those of the experimental trajectories. This led to the hypothesis that there was a significant difference in the fluid dynamics associated with linear swimming and turning. During the linear motion the body spins around the longitudinal axis

while in the turning motion there is no spinning; from our results we hypothesized that are key changes in the resulting fluid dynamics associated with this type of motion. This problem is encountered by other models and as was noted earlier the introduction of the correction factor α is used to accurately characterize the resulting torque on the cell body at low Reynold's number (13). In this work we hypothesized that the spinning of the cell reduces the drag the body experiences. This claim is collaborated by recent work that shows the rotation of uniquely shaped bodies in the same type of environment lead to increased propulsion efficiency (85, 86). Even though we could not identify the direct effect the spinning of the body has on the propulsion of the cell, our results provide evidence that this sort of rotation could lead to the maximization of energy at low Reynold's number.

This work also led to the ability to compare the multi-flagellated propulsion of *T. foetus* in relation to other microorganisms with varying strategies for generating low Reynold's number propulsion. The *T. foetus*'s propulsive force output during the recovery stroke (20-26 pN) is similar to those obtained for other eukaryotic flagellates. Even though the sperm exhibits a sinuisodal waveform and the *Chlamydomonas* has a cilary beating pattern, their propulsive force are within the same range, 13.5-25 pN (22, 89, 90). Also the propulsive force per flagella are within the range of other eukaryotic cells: the flagella of sperm, 6.5-11.1 pN (94), *Chlamydomonas reinhardti*, 2.4 pN (95), and *Volvox carteri*, 0.3-0.8 pN (95). Due to the fact that the total propulsive force generated by the *T. foetus* is comparable to the force generated by the biflagellate *Chlamydomonas* and uniflagellated sperm, we hypothesize that higher thrust generation is not necessarily the goal of multi-flagellated propulsion, but these strategies result in greater maneuverability or sensing. In previous work on *Giardia lamblia*, it is noted that the presence of multiple flagella pairs may aid in precise steering, orientation, and stability (34), this

same phenomenon can be observed in the *T.foetus*, with the recurrent flagella responsible for angular deviation, while the anterior flagella are responsible for forward propulsion.

In Chapter 2, the goal was to find out if the RFT method was the more accurate method for analyzing multi-flagellated propulsion. It was compared to the RSM method which was known to be more accurate for uni-flagellated cells. The RSM method was supposed to be more accurate than RFT due to the fact it takes into account the flagella-flagella and body-flagella hydrodynamic interactions while the Original RFT neglects it. However in this study we use a modified RFT model that does not use the standard equations to obtain the drag coefficients (C_N and C_T). But instead use a minimization of error procedure to fit the trajectory thus inherently accounting for the hydrodynamic interactions. In this manner it provides a better approximation than both the original RFT and RSM. It performs better in both swimming motions in both the angular and linear components. So with these results it was decided to use the RFT in 3-D analysis of the *T.foetus* body and flagella kinematics.

In Chapter 3, multi-flagellated propulsion was examined using a high speed 3-D platform and a 3-D resistive force theory (RFT) based model, with the *T.foetus* serving as a test case. Digital Holographic Microscopy was used to produce the 3-D trajectory of the *T.foetus* for the first time. Also for the first time, a 3D beating pattern of the flagella was generated by finding flagella beat forms that closely matched the cell's trajectory using the mean squared error values as a guide. This allowed for more accurate quantitative measurements and analysis of the forces caused by the flagella and their effect on the body as opposed to the previously acquired 2-D pattern. Along with the body coordinates and flagella beating patterns, this is the first time applying RFT in 3D for a multi-flagellated micro-organism, and with this we were able to further characterize and distinguish between the two distinct beating patterns that produce linear swimming and

turning. The major area of significance for the extension to 3-D is the ability to accurately track the trajectory of these cells, prior to this data, only planar motions can be analyzed and thus severely limiting knowledge of these organisms.

In the linear swimming motion, all four flagella generated a total of 41.75 pN of thrust. The Anterior flagella thrust values showed a similar cyclical characteristic when compared to the values of the 2-D case(105), with the free flagella providing 68% of anterior flagella thrust during the first third of the swimming motion, then the first stalked providing 50% of the anterior flagella thrust for the second third of the motion and finally the second stalked flagella contributing 45% of the anterior flagella thrust during the last third of the motion. When analyzing the force output of the recurrent flagellum, we see that it only is responsible for 6% of the forward thrust (along the x-axis of the body-aligned frame), 22% of the forward thrust of the body in the z-axis but provides 79% of the force in the y-axis of the body-aligned frame. When analyzing the force contributions of the flagella in the x-direction it is clear to see the cyclical nature of the contributions, the free flagellum dominate the force output for the first third of the cycle followed by the first stalked for the next third with the second stalk opposing the forward motion in this direction and then the second stalked for the last third. The recurrent flagellum produces minimal values and even proceeds to oppose the forward motion for the last third of the cycle. In the y-direction, the pattern is less distinguishable. The recurrent flagellum steadily drives the cell forward with each anterior flagella alternating between contributing towards the forward motion and opposing it. In the z-direction, the free and recurrent flagella contribute to the forward motion and their forces are slightly greater than that of the stalked flagella whose forces oppose the motion. This analysis shows the highly coordinated and balancing contributions that each flagella produce towards the movement of the body in this motion.

During the entire course of the swimming motion, the recurrent flagella provided the most total thrust, with the first stalked providing the second most, then the free and then the second stalked (**Table 1)**. The total thrust output of 41.75 pN seems significantly greater than the thrust output we got for the 2-D case, but this is misleading. The duration of the propulsive beat is different in both cases; .2s in this work compared to .255s in the previous work. When the time is normalize to mimic that of the previous work, the total force output is 32.75pN. This is still greater than the reported 20.69pN of the previous work. The extra force can be attributed to the added z-direction forces and the extended beating duration of the free and first stalked flagella.

In the case of the turning motion, all four flagella generated a total of 79.98 pN. When the duration of the beat was normalized to match that of our previous study, the total thrust output was 32.9pN compared to the previous value of 26.09pN. As in the case of the linear motion, the anterior flagella thrust values trended together with the previously discovered values in the 2-D case(105), the free flagella produces 64% of the anterior flagella thrust for the first third of the motion, but then its contribution significantly reduces to 21%, and by the last third its force contribution is opposite that of the motion of the cell. The free flagella seems to stop during the second third of the motion and beat very slightly in the opposite direction during the last part of the motion, this backward beating allowed for the model to match the cell's z and angular trajectory. The two stalked flagella intuitively exhibit similar thrust values throughout the cycle due to their similar beat form. In this motion the recurrent flagellum opposes the forward thrust in the z-direction, it contributes 20% of the x-axis thrust while contributing 64% of the y-axis thrust. In the x-direction, the free flagella dominate the first third of the force output and the stalked flagella dominate the rest of the motion with the recurrent producing minimal values. In the y-direction, the recurrent flagellum is the major driving force for the forward motion with the

anterior flagella contributing significantly less to the forward motion. The free flagellum actually opposes the motion during the last third of the motion. In the z-direction, the free flagellum solely contributes to the forward motion while the other three oppose it. Like for the linear motion the turning motion shows a highly coordinated contribution from each flagella towards the forward movement of the body in all three directions. Cumulatively, the recurrent flagella produced the most thrust during the turning motion, while the free produced the least and the two stalked exhibited similar total thrust values.

Using this model the Energy dissipated by the flagella can be compared for both swimming motions of the cell. We normalized both motions so that they had the same duration so as to be able to correctly compare the energy dissipation difference from the two different motions. This way the only difference between both motions was the flagella beat pattern and nothing else. The turning motion dissipated a total of 97.95J with the recurrent flagellum dissipating the most energy (41.59 J) and the anterior flagella all having relatively similar values. It also exhibited the same time coordinated cyclical characteristic that the thrust values possessed. The linear motion dissipated approximately twice as much energy as the turning (184.73 J) with the recurrent flagellum once again dissipating the most energy (61.56 J). The free flagella and stalked two exhibit similar values at 32.85 J and 33.73 J respectively, but the first stalked flagella this time does not trend with the other two anterior flagella (56.86 J). An intuitive explanation for the difference between the energy dissipation values is that in the linear swimming motion, the flagella cover more distance than in the turning. For the linear motion; in the x-direction, the energy dissipation is dominated by the anterior flagella, first by the free then the first stalked and then the second stalked. In the y-direction, the first stalked initially dissipates the most energy then the recurrent dominates the latter part of the motion. The free flagellum and second stalked

flagella dissipate relatively insignificant energy when compared to the other two. In the z-direction, the free and first stalked flagella dominate the energy dissipation with the other two dissipating significantly less energy. When the turning motion is analyzed; in the x-direction, the free flagellum dissipates the most energy at the beginning of the motion then the stalked flagella dominate towards the end. In the y-direction, the recurrent flagellum dominates the energy dissipation by far, rendering the energy dissipation from the anterior flagella insignificant. And in the z-direction, the pattern in the y-axis is repeated except that this time it is the free flagellum dissipating the energy and the other three being insignificant. The energy results highlight the difference in beat pattern of the flagella during these two motions; suggesting the possibility of *T.foetus* actively responding to environmental cues and changing its beat pattern due to them similar to the "run and tumble" strategies of bacteria(11, 78, 79, 81) and *Chlamydomonas*(16).

The huge energy difference due largely to the change in direction of the first stalked flagella leads to interesting biological implications that would not have been noticed without the implementation of the model. As explained earlier and shown in **Fig. 3.2** the first stalked flagella covers more ground in the linear motion by beating in the opposite direction of its turning motion. This sort of change in direction leads to the hypothesis that a change in twisting of the central pair microtubules might be responsible for this. It is already known that in *Chlamydomonas* different waveforms led to differential twisting in each beat form (72). This sort of phenomenon could be caused by activation of specialized dynein motors, through calcium gradients or mechanical feedback, that result in central pair twisting (72).

The ability to correctly estimate the thrust and energy dissipation contributions of each flagella leads to very exciting opportunities. First, these forces can be used to correctly derive and analyze the details of dynein activity in the flagella. This would result in better understanding of

pathogens and lead to possible treatments for trichomoniasis and other pathogen related maladies. Another use for this ability is in the area of bio-robotics. This work will aid in understanding general principles of multi-flagellated propulsion and insights from this study will serve as inspiration for medical bio-robot designs; due to the fact that the bio-robots would be of similar size and will have to navigate similar environments as the microorganism. Due to the robust use of flagella and cilia-like organelles as propulsive structures in swimming microorganisms, the fluid mechanics involved in locomotion of microorganisms has received significant attention for its practical use in micro-robot design (112-114).

Recommendation For Future Work

Although the work presented has demonstrated the effectiveness of this approach in the analysis of 3-D multi-flagellated propulsion, there are still some areas that could be improved on.

Acquiring Experimental Flagella Position

In the 2-D dimensional analysis of the *T.foetus* propulsion, it was possible to get the actual experimental position of the flagella and conduct the analysis on them. But in the 3-D analyses we had to generate the 3-D positions from the existing 2-D positions. A next step should be to acquire the actual positions of these flagella. This is difficult due to the relative small width of the flagella compared to that of the body and the similar refractive index of the flagella and the media. Possible solutions could be to modify the ingredients of the media so as to change the refractive index without killing or retarding the motion of the cell. Having these experimental positions would lead to more accurate analyses of this cell.

Developing Model Capable of Simulating Different Flagella Configurations and Beating Patterns

Currently the model used in this study can only analyze already existing motions of the cell; it requires the linear and angular velocity of the cell as inputs in other to be able to produce

the trajectory, thrust and energy values. Developing a model that by-passes this requirement will lead to the ability to arbitrarily change the motion of one or more flagella and analyze the effect on the overall motion of the cell. From these simulations the role of each flagella can specifically be understood. The huge obstacle in accomplishing this goal is the asymmetric waveform of the flagella. Work that has been done to simulate trajectory of flagellated organisms has been done with organisms possessing flagella with mathematically describable waveforms like the sinusoidal beating sperm flagella or the helical motions of bacteria flagella. Currently the beating pattern of the *T.foetus* and other eukaryotic cells with similar beating flagella cannot be accurately described mathematically and thus models that simulate cell motions like the chain-link models(35) and other modified RFT models(25) cannot be used. This particular problem of mathematically describing the flagella waveform accurately has resulted in the lack of models being able to simulate the motion of eukaryotes with similar flagella waveforms. Gueron and Levit-Gurevich were able to model a ciliary waveform for their breakthrough work on modelling ciliary motion(65, 116); even though the motion might not be exactly that of the *T.foetus* flagella, it could serve as a good approximation to run simulations with. If the flagella beat form can be characterized, an iterative procedure could be used to predict the motion of the cell body with knowing the initial velocity of the body.

List of References

1. Batchelor GK (1992) An introduction to fluid-dynamics - A citation-classic commentary on an introduction to fluid-dynamics by Batchelor, G.K. *Current Contents/Physical Chemical & Earth Sciences* (40):8-8.
2. Cohen N & Boyle JH (2010) Swimming at low Reynolds number: a beginners guide to undulatory locomotion. *Contemporary Physics* 51(2):103-123.
3. Purcell EM (1977) Life at low Reynolds number. *Am. J. Phys.* 45(1):3-11.
4. Pozrikidis C (1992) *Boundary integral and singularity methods for linearized viscous flow* (Cambridge University Press).
5. Lauga E (2011) Life around the scallop theorem. *Soft Matter* 7(7):3060-3065.
6. Blair DF & Dutcher SK (1992) Flagella in prokaryotes and lower eukaryotes. *Current Opinion in Genetics & Development* 2(5):756-767.
7. Behkam B & Sitti M (2006) Design Methodology for Biomimetic Propulsion of Miniature Swimming Robots. *J. Dyn. Syst.-T ASME.* 128(1):36-43.
8. Amos LA & Amos WB (1991) *Molecules of the Cytoskeleton* (Guilford Press, New York).
9. Gibbons IR (1981) Cilia and flagella of eukaryotes. *J. Cell Bio.* 91(3):107-124.
10. Watari N & Larson RG (2010) The Hydrodynamics of a Run-and-Tumble Bacterium Propelled by Polymorphic Helical Flagella. *Biophysical Journal* 98(1):12-17.
11. Stocker R (2011) Reverse and flick: Hybrid locomotion in bacteria. *Proceedings of the National Academy of Sciences* 108(7):2635-2636.
12. Taylor BL & Koshland DE (1974) Reversal of Flagellar Rotation in Monotrichous and Peritrichous Bacteria: Generation of Changes in Direction. *Journal of Bacteriology* 119(2):640-642.
13. Bayly PV*, et al.* (2011) Propulsive Forces on the Flagellum during Locomotion of Chlamydomonas reinhardtii. *Biophysical Journal* 100(11):2716-2725.
14. Brokaw CJ, Luck DJ, & Huang B (1982) Analysis of the movement of Chlamydomonas flagella:" the function of the radial-spoke system is revealed by comparison of wild-type and mutant flagella. *The Journal of Cell Biology* 92(3):722-732.
15. Bloodgood RA (1977) Motility occurring in association with the surface of the Chlamydomonas flagellum. *The Journal of Cell Biology* 75(3):983-989.
16. Polin M, Tuval I, Drescher K, Gollub JP, & Goldstein RE (2009) Chlamydomonas Swims with Two “Gears” in a Eukaryotic Version of Run-and-Tumble Locomotion. *Science* 325(5939):487-490.
17. Taylor G (1951) Analysis of the Swimming of Microscopic Organisms. *Proceedings of the Royal Society of London. Series A. Mathematical and Physical Sciences* 209(1099):447-461.
18. Hancock GJ (1953) The self-propulsion of microscopic organisms through liquids *Proceedings of the Royal Society of London Series a-Mathematical and Physical Sciences* 217(1128):96-121.
19. Gray J & Hancock G (1955) The propulsion of sea-urchin spermatozoa. *J. Exp. Biol.* 32(4):802-814.
20. Lighthill J (1976) Flagellar Hydrodynamics: The John von Neumann Lecture, 1975. *SIAM Review* 18(2):161-230.
21. Johnson RE & Brokaw CJ (1979) Flagellar hydrodynamics. A comparison between resistive-force theory and slender-body theory. *Biophysical Journal* 25(1):113-127.

22. Ishijima S (2011) Dynamics of flagellar force generated by a hyperactivated spermatozoon. *Reproduction* 142(3):409-415.
23. Gillies EA, Cannon RM, Green RB, & Pacey AA (2009) Hydrodynamic propulsion of human sperm. *Journal of Fluid Mechanics* 625:445-474.
24. Cisneros LH, Cortez R, Dombrowski C, Goldstein RE, & Kessler JO (2007) Fluid dynamics of self-propelled microorganisms, from individuals to concentrated populations. *Experiments in Fluids* 43(5):737-753.
25. Rodenborn B, Chen C-H, Swinney HL, Liu B, & Zhang HP (2013) Propulsion of microorganisms by a helical flagellum. *Proceedings of the National Academy of Sciences* 110(5):E338–E347.
26. Cortez R (2001) The Method of Regularized Stokeslets. *SIAM Journal on Scientific Computing* 23(4):1204-1225.
27. Cortez R, Fauci L, & Medovikov A (2005) The method of regularized Stokeslets in three dimensions: Analysis, validation, and application to helical swimming. *Physics of Fluids (1994-present)* 17(3):-.
28. Gookin JL, Birkenheuer AJ, Breitschwerdt EB, & Levy MG (2002) Single-tube nested PCR for detection of Tritrichomonas foetus in feline feces. *Journal of Clinical Microbiology* 40(11):4126-4130.
29. Midlej V, Pereira-Neves A, Kist LW, Bogo MR, & Benchimol M (2011) Ultrastructural features of Tritrichomonas mobilensis and comparison with Tritrichomonas foetus. *Veterinary Parasitology* 182(2-4):171-180.
30. Frey CF & Muller N (2012) Tritrichomonas - Systematics of an enigmatic genus. *Molecular and Cellular Probes* 26(3):132-136.
31. Bryan LA, Campbell JR, & Gajadhar AA (1999) Effects of temperature on the survival of Tritrichomonas foetus in transport, diamond's and InPouch TF media. *Veterinary Record* 144(9):227-232.
32. Rae DO (1989) Impact of Trichomoniasis on the Cow Calf Producers Profitability. *Journal of the American Veterinary Medical Association* 194(6):771-775.
33. Gookin JL, Breitschwerdt EB, Ley MG, Gager RB, & Benrud JG (1999) Diarrhea associated with trichomonosis in cats. *Journal of the American Veterinary Medical Association* 215(10):1450-1454.
34. Lenaghan SC, Davis CA, Henson WR, Zhang ZL, & Zhang MJ (2011) High-speed microscopic imaging of flagella motility and swimming in Giardia lamblia trophozoites. *Proceedings of the National Academy of Sciences of the United States of America* 108(34):E550-E558.
35. Lenaghan SC, Chen J, & Zhang M (2013) Modeling and analysis of propulsion in the multiflagellated micoorganism Giardia lamblia. *Physical Review E* 88(1):012726.
36. Singh BN, Lucas JJ, Beach DH, Shin ST, & Gilbert RO (1999) Adhesion of Tritrichomonas foetus to Bovine Vaginal Epithelial Cells. *Infection and Immunity* 67(8):3847-3854.
37. Corbeil LB*, et al.* (1989) Adherence of Tritrichomonas foetus to bovine vaginal epithelial cells. *Infection and Immunity* 57(7):2158-2165.
38. Monteavaro CE*, et al.* (2007) Interaction of Tritrichomonas foetus with the reproductive tract of experimentally infected female BALB/c mice: Ultrastructural evaluation. *The Veterinary Journal* 173(1):204-208.

39. Meyer Mariante R, Coutinho Lopes L, & Benchimol M (2004) Tritrichomonas foetus pseudocysts adhere to vaginal epithelial cells in a contact-dependent manner. *Parasitology Research* 92(4):303-312.
40. Stockdale HD*, et al.* (2008) Experimental infection of cats (Felis catus) with Tritrichomonas foetus isolated from cattle. *Veterinary Parasitology* 154(1–2):156-161.
41. Gookin JL*, et al.* (2001) Experimental infection of cats with Tritrichomonas foetus. *American Journal of Veterinary Research* 62(11):1690-1697.
42. BonDurant RH (1997) Pathogenesis, diagnosis, and management of trichomoniasis in cattle. *The Veterinary clinics of North America. Food animal practice* 13(2):345-361.
43. Benchimol M, Andrade Rosa I, Silva Fontes R, & Burla Dias Â (2008) Trichomonas adhere and phagocytose sperm cells: adhesion seems to be a prominent stage during interaction. *Parasitology Research* 102(4):597-604.
44. Monteiro-Leal LH, Farina M, Benchimol M, Kachar B, & De Souza W (1995) Coordinated Flagellar and Ciliary Beating in the Protozoon *Tritrichomonas foetus*. *Journal of Eukaryotic Microbiology* 42(6):709-714.
45. Woodrum DT & Linck RW (1980) Structural Basis of Motility in the Microtubular Axostyle - Implications for Cytoplasmic Microtubule Structure and Function. *Journal of Cell Biology* 87(2):404-414.
46. Monteiro-Leal LH, Farina M, & de Souza W (1996) Free movement of *Tritrichomonas foetus* in a liquid medium: A video-microscopy study. *Cell Motility and the Cytoskeleton* 34(3):206-214.
47. Rüffer U & Nultsch W (1985) High-speed cinematographic analysis of the movement of Chlamydomonas. *Cell Motility* 5(3):251-263.
48. Bayly PV, Lewis BL, Kemp PS, Pless RB, & Dutcher SK (2010) Efficient spatiotemporal analysis of the flagellar waveform of *Chlamydomonas reinhardtii*. *Cytoskeleton* 67(1):56-69.
49. Okuno M & Hiramoto Y (1979) Direct Measurements of the Stiffness of Echinoderm Sperm Flagella. *Journal of Experimental Biology* 79(1):235-243.
50. Chen J, Lenaghan SC, & Mingjun Z (2012) Analysis of dynamics and planar motion strategies of a swimming microorganism *Giardia lamblia*. *Robotics and Automation (ICRA), 2012 IEEE International Conference on*, pp 4204-4209.
51. Spagnolie SE & Lauga E (2010) The optimal elastic flagellum. *Physics of Fluids* 22(3):031901-031915.
52. de Souza W & Rocha GM (2011) Atomic force microscopy: a tool to analyze the structural organization of pathogenic protozoa. *Trends in Parasitology* 27(4):160-167.
53. Dvorak JA*, et al.* (2000) The application o f the atomic force microscope to studies of medically important protozoan parasites. *Journal of Electron Microscopy* 49(3):429-435.
54. Rocha GM, Miranda K, Weissmüller G, Bisch PM, & de Souza W (2008) Ultrastructure of Trypanosoma cruzi revisited by atomic force microscopy. *Microscopy Research and Technique* 71(2):133-139.
55. Chen X, Woo K, & Injeti E (2012) Atomic Force Microscopy Studies of Ciliary Structures of Tetrahymena Themophila. *Microscopy and Microanalysis* 18(SupplementS2):264-265.
56. Franke O*, et al.* (2007) Mechanical properties of hyaline and repair cartilage studied by nanoindentation. *Acta Biomaterialia* 3(6):873-881.

57. Ishijima S & Hiramoto Y (1994) Flexural Rigidity of Echinoderm Sperm Flagella. *Cell Structure and Function* 19(6):349-362.
58. Baba SA (1972) Flexural Rigidity and Elastic Constant of Cilia. *Journal of Experimental Biology* 56(2):459-467.
59. Fujime S, Maruyama M, & Asakura S (1972) Flexural rigidity of bacterial flagella studied by quasielastic scattering of laser light. *Journal of Molecular Biology* 68(2):347-359.
60. Schwartz EA, Leonard ML, Bizios R, & Bowser SS (1997) Analysis and modeling of the primary cilium bending response to fluid shear. *American Journal of Physiology - Renal Physiology* 272(1):F132-F138.
61. Gray J & Hancock GJ (1955) The Propulsion of Sea-Urchin Spermatozoa. *Journal of Experimental Biology* 32(4):802-814.
62. Yundt A, Shack W, & Lardner T (1975) Applicability of hydrodynamic analyses of spermatozoan motion. *The Journal of Experimental Biology* 62(1):27-41.
63. Brokaw CJ (1970) Bending Moments in Free-Swimming Flagella. *Journal of Experimental Biology* 53(2):445-464.
64. Winet H & Keller SR (1976) Spirillum swimming: theory and observations of propulsion by the flagellar bundle. *Journal of Experimental Biology* 65(3):577-602.
65. Gueron S & Liron N (1992) Ciliary Motion Modeling, and Dynamic Multicilia Interactions. *Biophysical Journal* 63(4):1045-1058.
66. Friedrich BM, Riedel-Kruse IH, Howard J, & Jülicher F (2010) High-precision tracking of sperm swimming fine structure provides strong test of resistive force theory. *The Journal of Experimental Biology* 213(8):1226-1234.
67. Takano Y, Yoshida K, Kudo S, Nishitoba M, & Magariyama Y (2003) Analysis of Small Deformation of Helical Flagellum of Swimming *Vibrio alginolyticus*. *JSME International Journal Series C Mechanical Systems, Machine Elements and Manufacturing* 46(4):1241-1247.
68. Johnson RE & Brokaw CJ (1979) Flagellar Hydrodynamics - Comparison Between Resistive Force Theory and Slender Body Theory. *Biophysical Journal* 25(1):113-127.
69. Holwill MEJ & Sleigh MA (1967) Propulsion by Hispid Flagella. *Journal of Experimental Biology* 47(2):267-276.
70. Hyams JS & Borisy GG (1978) Isolated flagellar apparatus of Chlamydomonas: characterization of forward swimming and alteration of waveform and reversal of motion by calcium ions in vitro. *Journal of Cell Science* 33(1):235-253.
71. Bessen M, Fay R, & Witman G (1980) Calcium control of waveform in isolated flagellar axonemes of chlamydomonas. *The Journal of Cell Biology* 86(2):446-455.
72. Mitchell DR (2003) Orientation of the central pair complex during flagellar bend formation in Chlamydomonas. *Cell Motility and the Cytoskeleton* 56(2):120-129.
73. Ralston KS, Kabututu ZP, Melehani JH, Oberholzer M, & Hill KL (2009) The Trypanosoma brucei Flagellum: Moving Parasites in New Directions. *Annual Review of Microbiology* 63(1):335-362.
74. Berg HC & Turner L (1990) Chemotaxis of bacteria in glass capillary arrays. Escherichia coli, motility, microchannel plate, and light scattering. *Biophysical Journal* 58(4):919-930.

75. Rüffer U & Nultsch W (1990) Flagellar photoresponses of Chlamydomonas cells held on micropipettes: I. Change in flagellar beat frequency. *Cell Motility and the Cytoskeleton* 15(3):162-167.
76. Benchimol M, Elias CA, & Souza Wd (1981) Specializations in the Flagellar Membrane of Tritrichomonas foetus. *The Journal of Parasitology* 67(2):174-178.
77. Rhyan JC, Blanchard PC, Kvasnicka WG, Hall MR, & Hanks D (1995) Tissue-invasive Tritrichomonas foetus in four aborted bovine fetuses. *Journal of Veterinary Diagnostic Investigation* 7(3):409-412.
78. Clark DA & Grant LC (2005) The bacterial chemotactic response reflects a compromise between transient and steady-state behavior. *Proceedings of the National Academy of Sciences of the United States of America* 102(26):9150-9155.
79. Kearns DB & Shimkets LJ (1998) Chemotaxis in a gliding bacterium. *Proceedings of the National Academy of Sciences* 95(20):11957-11962.
80. Berg HC & Turner L (1995) Cells of Escherichia coli swim either end forward. *Proceedings of the National Academy of Sciences* 92(2):477-479.
81. Yuan J, Fahrner KA, Turner L, & Berg HC (2010) Asymmetry in the clockwise and counterclockwise rotation of the bacterial flagellar motor. *Proceedings of the National Academy of Sciences* 107(29):12846-12849.
82. Hill KL (2003) Biology and Mechanism of Trypanosome Cell Motility. *Eukaryotic Cell* 2(2):200-208.
83. Weiße S*, et al.* (2012) A Quantitative 3D Motility Analysis of *Trypanosoma brucei* by Use of Digital In-line Holographic Microscopy. *PLoS ONE* 7(5):e37296.
84. Allena R & Aubry D (2012) 'Run-and-tumble' or 'look-and-run'? A mechanical model to explore the behavior of a migrating amoeboid cell. *Journal of Theoretical Biology* 306(0):15-31.
85. Spagnolie SE, Liu B, & Powers TR (2013) Locomotion of Helical Bodies in Viscoelastic Fluids: Enhanced Swimming at Large Helical Amplitudes. *Physical Review Letters* 111(6):068101.
86. Liu B, Powers TR, & Breuer KS (2011) Force-free swimming of a model helical flagellum in viscoelastic fluids. *Proceedings of the National Academy of Sciences* 108(49):19516-19520.
87. Celli JP*, et al.* (2009) Helicobacter pylori moves through mucus by reducing mucin viscoelasticity. *Proceedings of the National Academy of Sciences* 106(34):14321-14326.
88. Su T-W*, et al.* (2013) Sprem Trajectories from Chiral Ribbons. *Scientific Reports* 3.
89. Hollm J, Khan R, Marongelli E, & Guilford W (2009) Laser Trap Characterization and Modeling of Phototaxis in Chlamydomonas reinhardtii. *Cel. Mol. Bioeng.* 2(2):244-254.
90. Baltz JM, Katz DF, & Cone RA (1988) Mechanics of sperm-egg interaction at the zona pellucida. *Biophysical Journal* 54(4):643-654.
91. Chattopadhyay S, Moldovan R, Yeung C, & Wu XL (2006) Swimming efficiency of bacterium *Escherichia coli*. *Proceedings of the National Academy of Sciences* 103(37):13712-13717.
92. Hughes MP & Morgan H (1999) Measurement of bacterial flagellar thrust by negative dielectrophoresis. *Biotechnology Progress* 15(2):245-249.
93. Kuroda K & Kamiya N (1989) Propulsive force of Paramecium as revealed by the video centrifuge microscope. *Experimental Cell Research* 184(1):268-272.

94. Green DPL (1988) Sperm Thrusts and the Problem of Penetration. *Biological Reviews* 63(1):79-105.
95. Cristian A. Solari, John O. Kessler, & Richard E. Michod (2006) A Hydrodynamics Approach to the Evolution of Multicellularity: Flagellar Motility and Germ-Soma Differentiation in Volvocalean Green Algae. *The American Naturalist* 167(4):537-554.
96. Darnton NC, Turner L, Rojevsky S, & Berg HC (2007) On Torque and Tumbling in Swimming *Escherichia coli*. *Journal of Bacteriology* 189(5):1756-1764.
97. Chwang AT & Wu TYT (1975) Hydromechanics of Low-Reynolds Number Flow .2. Singularity Method for Stokes Flow. *Journal of Fluid Mechanics* 67(FEB25):787-815.
98. Lighthill MJ (1952) On the squirming motion of nearly spherical deformable bodies through liquids at very small reynolds numbers. *Communications on Pure and Applied Mathematics* 5(2):109-118.
99. Brennen C & Winet H (1977) Fluid Mechanics of Propulsion by Cilia and Flagella. *Annual Review of Fluid Mechanics* 9(1):339-398.
100. Gibbons IR (1981) Cilia and Flafella of Eukaryotes. *Journal of Cell Biology* 91(3):S107-S124.
101. Lindemann CB (1994) A model of flagellar and ciliary functioning which uses the forces transverse to the axoneme as the regulator of dynein activation. *Cell Motility and the Cytoskeleton* 29(2):141-154.
102. Gennerich A, Carter AP, Reck-Peterson SL, & Vale RD (Force-Induced Bidirectional Stepping of Cytoplasmic Dynein. *Cell* 131(5):952-965.
103. Higdon JJL (1979) A hydrodynamic analysis of flagellar propulsion. *Journal of Fluid Mechanics* 90(04):685-711.
104. Singleton J, Diller E, Andersen T, Regnier S, & Sitti M (2011) Micro-scale propulsion using multiple flexible artificial flagella. *Intelligent Robots and Systems (IROS), 2011 IEEE/RSJ International Conference on*, pp 1687-1692.
105. Lenaghan S. C. N-VS, Reese BE, Zhang M. (2014) Unlocking the secrets of multi-flagellated propulsion: drawing insights from *Tritrichomonas foetus*. *J. R. Soc. Interface* 20131149.
106. Lenaghan SC, Davis CA, Henson WR, Zhang Z, & Zhang M (2011) High-speed microscopic imaging of flagella motility and swimming in Giardia lamblia trophozoites. *Proceedings of the National Academy of Sciences* 108(34):E550–E558.
107. Pertuz S, Puig D, & Garcia MA (2013) Analysis of focus measure operators for shape-from-focus. *Pattern Recognition* 46(5):1415-1432.
108. Chwang AT & Wu TYT (1975) Hydromechanics of Low-Reynolds-Number Flow. 2. Singularity Method for Stokes Flows. *Journal of Fluid Mechanics* 67(FEB25):787-815.
109. Sheng J*, et al.* (2007) Digital holographic microscopy reveals prey-induced changes in swimming behavior of predatory dinoflagellates. *Proceedings of the National Academy of Sciences* 104(44):17512-17517.
110. Wilson LG, Carter LM, & Reece SE (2013) High-speed holographic microscopy of malaria parasites reveals ambidextrous flagellar waveforms. *Proceedings of the National Academy of Sciences*.
111. Chattopadhyay S, Moldovan R, Yeung C, & Wu XL (2006) Swimming efficiency of bacterium Escherichiacoli. *Proceedings of the National Academy of Sciences* 103(37):13712-13717.

112. Soong RK*, et al.* (2000) Powering an inorganic nanodevice with a biomolecular motor. *Science* 290(5496):1555-1558.
113. Martel S, Mohammadi M, Felfoul O, Lu Z, & Pouponneau P (2009) Flagellated Magnetotactic Bacteria as Controlled MRI-trackable Propulsion and Steering Systems for Medical Nanorobots Operating in the Human Microvasculature. *International Journal of Robotics Research* 28(4):571-582.
114. Nelson BJ, Kaliakatsos IK, & Abbott JJ (2010) Microrobots for Minimally Invasive Medicine. *Annual Review of Biomedical Engineering, Vol 12,* Annual Review of Biomedical Engineering, eds Yarmush ML, Duncan JS, & Gray ML (Annual Reviews, Palo Alto), Vol 12, pp 55-85.
115. Magdanz V, Sanchez S, & Schmidt OG (2013) Development of a Sperm-Flagella Driven Micro-Bio-Robot. *Advanced Materials* 25(45):6581-6588.
116. Gueron S & Levit-Gurevich K (2001) A three–dimensional model for ciliary motion based on the internal 9 + 2 structure. *Proceedings of the Royal Society of London. Series B: Biological Sciences* 268(1467):599-607.

Vita

Stefan Nwandu-Vincent was born in Washington D.C., to the parents of Steve and Nkem Nwandu in 1988. He attended Redeemers International School in Lagos, Nigeria for his Nursery and Primary School. He then proceeded to Redeemers International Secondary School for his secondary studies. He returned to America to attend Francis Hammond Middle school in Alexandria, Virginia for the last half of middle school. Then moved south to Knoxville, Tennessee and attended Bearden High School. He stayed in Knoxville to attend the University of Tennessee and major in Biomedical Engineering. He loved his undergraduate experience in Knoxville so much that he decided to pursue and complete his doctoral degree in Biomedical Engineering at The University of Tennessee.